J. Fluid Mech. (1984), *vol.* 147, *pp.* 261–289
Printed in Great Britain

Secondary flows in a plane channel: their relationship and comparison with turbulent flows

By B. L. ROZHDESTVENSKY AND I. N. SIMAKIN
Keldysh Institute of Applied Mathematics, Academy of Sciences of the USSR, Miusskaja Sq. 4, Moscow 125047, USSR

(Received 19 April 1982 and in revised form 24 May 1984)

Two- and three-dimensional non-stationary viscous-fluid flows in a plane channel are considered. By means of efficient computational algorithms for direct integration of the incompressible Navier–Stokes equations the evolution of these flows over large time intervals is simulated. Classes of two- and three-dimensional non-stationary flows with stationary integral characteristics (the flow rate, mean pressure gradient, total energy of pulsations etc.) were found. Such flows are called secondary flows. Two-dimensional secondary flows have only qualitative similarity to turbulent flows observed in experiments. Three-dimensional secondary flows agree very well, even quantitatively, with turbulent flows. The principal characteristics of turbulent flows such as drag coefficient, mean-velocity profile, the distributions of the pulsation velocity components and some others are reproduced in three-dimensional secondary flows with good accuracy.

1. Introduction

The behaviour of infinitesimal disturbances of plane Poiseuille flow has been investigated reasonably well (see e.g. Betchov & Criminale 1967; Drazin & Reid 1981). Problems concerning the evolution of finite-amplitude disturbances and more generally on the theory of nonlinear hydrodynamical stability have been studied far less exhaustively. A considerable number of works have been devoted to this problem. A survey of these works may be found in Stuart (1971), Shkadov (1973*a*), Stewartson (1974), Joseph (1976), Coldshtick & Stern (1977), Orszag & Kells (1980) and Herbert (1983).

Investigations presented in this paper can also be considered as studies of the evolution of finite-amplitude disturbances. However, our principal task is search for stable unsteady secondary flows, to examine and to compare them with experiment.

Usually two formulations of the problem of the evolution of incompressible viscous fluid flows in an infinite channel or pipe are applied. The first formulation assumes constancy of flux, while the second one assumes constancy of the space-averaged pressure gradient.

These two types of flow are characterized by different Reynolds numbers, usually denoted by the same symbol. Therefore comparison of the results obtained in the two different problem formulations at the same value of these Reynolds numbers leads to wrong conclusions. Let us briefly discuss this general question.†

† Some remarks on this question may be found also in Stuart (1960).

The flow in a plane channel is usually characterized by the Reynolds number

$$R = \frac{UL}{\nu}, \tag{1.1}$$

where U is the maximum fluid velocity, L is the half-channel width and ν is the kinematic viscosity. The formulae

$$R_Q = \frac{3Q}{8\nu\rho_0 L}, \tag{1.2}$$

$$R_p = \frac{|\nabla p| L^3}{2\rho_0 \nu^2} \tag{1.3}$$

produce for Poiseuille flow results identical with (1.1) if Q is taken as flow rate through a square plane surface with dimensions $2L \times 2L$ that is placed perpendicular to the flow between the channel walls; ∇p is the pressure gradient; ρ_0 is the fluid density, which is taken as constant.

Therefore, for Poiseuille flow $R_p = R_Q = R$, and we can depict any Poiseuille flow as the bisector point in the (R_Q, R_p)-plane.

In the case of an unsteady flow in a plane channel we shall understand $\nabla p(t)$ to be an instantaneous mean pressure gradient obtained by averaging over the whole space between the channel walls and $\boldsymbol{Q}(t)$ as an instantaneous flow-rate vector through the surface mentioned above. This vector is defined as $\boldsymbol{Q}(t) = 4L^2\rho_0 \boldsymbol{u}(t)$, where $\boldsymbol{u}(t)$ is the space-averaged flow velocity.

For a non-stationary flow in a plane channel we introduce two Reynolds numbers $R_Q(t)$ and $R_p(t)$. The number R_Q obtained by substituting $Q = |\boldsymbol{Q}(t)|$ into (1.2) will be denoted by $R_Q(t)$, similarly $R_p(t)$ is the result of substitution of $|\nabla p| = |\nabla p(t)|$ into (1.3).

In the first problem formulation a class of flows with fixed flow rate ($R_Q(t) = R_Q = \text{const}$) is considered. Therefore the number R_Q is called the Reynolds number of all steady and unsteady flows from this class.

In the second problem formulation ($\nabla p(t) = \text{const}$) the number $R_p = \text{const}$ is called the Reynolds number of all the flows under consideration.

Suppose there exists a flow for which both Reynolds numbers $R_p(t) = R_p$ and $R_Q(t) = R_Q$ are constant. The Reynolds number R_p appears to be equal to R_Q only for Poiseuille flow; for non-stationary flows $R_p > R_Q$.†

A non-stationary flow with constant Reynolds numbers R_Q and R_p ($R_p > R_Q$) will be called a secondary flow. This flow belongs simultaneously to both problem formulations described above. Thus the secondary flows obtained with different external conditions should be compared on the basis of either (but only one) Reynolds-number definition.

Note that the existence of secondary flows implies the instability of Poiseuille flow (to finite-amplitude disturbances at the subcritical Reynolds numbers).

There are a number of works concerned with the search for secondary flows in a plane channel. Most of them deal with the search for two-dimensional secondary flows that are periodic in the homogeneous spatial coordinate x with a period $X = 2\pi/\alpha_0$, α_0 being a minimal wavenumber.‡

† Thomas (1942) and Serrin (1959) have shown that, for flows in a tube which are statistically stationary and periodic in the downstream coordinate, $R_p > R_Q$. This conclusion may be easily extended to the case of a plane channel.

‡ Here and in what follows we take $L = 1$.

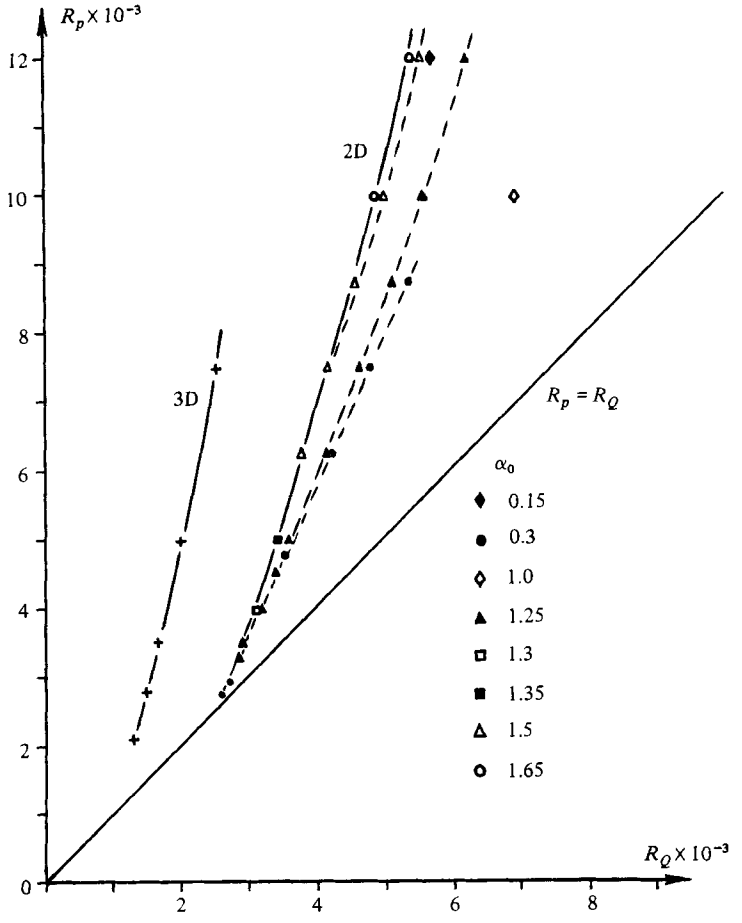

FIGURE 1. Secondary flows in the (R_Q, R_p)-plane. The curve 2D corresponds to two-dimensional limit secondary flows; curve 3D corresponds to three-dimensional secondary flows.

From numerical calculations of the solutions of the Navier–Stokes equations George, Hellums & Martin (1974) inferred that Poiseuille flow is unstable to two-dimensional finite-amplitude disturbances with $\alpha_0 = 1.05$ for $R_Q \geqslant 3500$. The authors note that they were not able to find non-decaying disturbances with $\alpha_0 \gtrsim 1$ for $R_Q < 3500$.

Zahn *et al.* (1974) investigated the question of existence of subcritical and supercritical two-dimensional secondary flows for a wide range of Reynolds numbers. The authors found instability of Poiseuille flow to finite-amplitude disturbances with wavenumber $\alpha_0 = 1.3126$ at $R_p = 2707$. They also drew the conclusion that Poiseuille flow is more stable to three-dimensional than to two-dimensional disturbances.

Herbert (1977) obtained approximate two-dimensional solutions of the Navier–Stokes equations periodic simultaneously in the x-coordinate and in time. The author concluded that such a solution exists for $R_p = 2935$ and $\alpha_0 = 1.3231$.

By means of direct numerical integration of the Navier–Stokes equations Orszag & Kells (1980) investigated the stability of Poiseuille flow to two-dimensional and three-dimensional finite-amplitude disturbances. On the basis of computations of

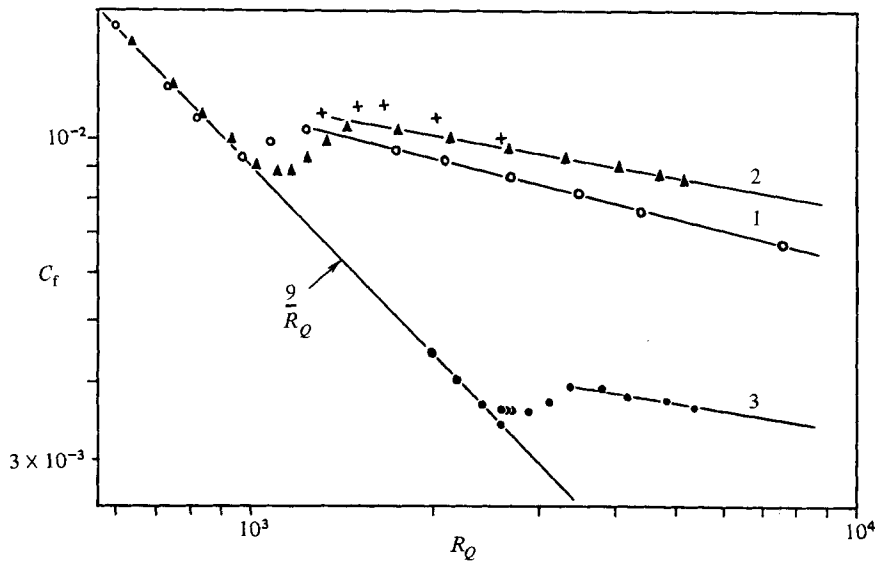

FIGURE 2. Drag coefficient C_f as a function of Reynolds number R_Q. Poiseuille flow: $C_f = 9/R_Q$. Experimental data: ○, Whan & Rothfus (1959) (curve 1, $C_f = 0.0618 R_Q^{-\frac{1}{4}}$); ▲, Patel & Head (1969) (curve 2, $C_f = 0.0358 R_Q^{-\frac{1}{4}}$). Results of our calculations: ●, two-dimensional limit secondary flows (curve 3, $C_f = 0.0153 R_Q^{-\frac{1}{4}}$); +, three-dimensional secondary flows.

evolution of finite-amplitude disturbances in very short time intervals $(0, T)$, $T = 100$–150, the authors stated that stable two-dimensional flows other than the Poiseuille flow exist when $R_p \gtrsim 2800$ and $\alpha_0 = 1.3231$. Three-dimensional computations of the evolution of disturbances were performed by them in still smaller time intervals. They observed 'the breakdown to turbulence' at the Reynolds numbers $R_p \gtrsim 1250$.

The development in time of small three-dimensional disturbances against a background of two-dimensional disturbances of Poiseuille flow was simulated numerically by Orszag & Patera (1980). It was found that when $R_p \gtrsim 1000$ the energy of small three-dimensional disturbances quickly grew exponentially. They studied also the evolution of three-dimensional finite-amplitude disturbances in a small time interval at $R_p = 5000$ (Orszag & Patera 1981) and generalized their results for Poiseuille and a number of other shear flows (Orszag & Patera 1983).

In the present paper the study of secondary flows and their comparison with turbulent flows are performed. By means of the numerical techniques developed, the flows with a fixed mean pressure gradient are simulated. Some classes of two- and three-dimensional secondary flows are obtained.

Two-dimensional secondary flows with the periodicity intervals $X \lesssim 2\pi$ ($\alpha_0 \gtrsim 1$) were found for Reynolds numbers $R_p \geqslant 3250$ ($R_Q \geqslant 2855$). In the range $R_p \geqslant 2750$ ($R_Q \geqslant 2612$) two-dimensional secondary flows with $X \gtrsim 6\pi$ ($\alpha_0 \lesssim 0.3$) were discovered.

Three-dimensional secondary flows were found for $R_p \geqslant 2100$ ($R_Q \geqslant 1313$). It should be pointed out that three-dimensionality of pulsations considerably increases the drag (reduces the flow rate Q).

Each secondary flow may be depicted by a point in the (R_Q, R_p)-plane. The secondary flows computed are shown in figure 1. Curve 2D, which we call 'the limiting curve', corresponds to the secondary flows in which the maximal drag (at fixed flux)

or minimal flux (at fixed mean pressure gradient) are realized. This limiting curve is also plotted in the (R_Q, C_f)-plane (C_f being the drag coefficient; figure 2). The computed three-dimensional secondary flows, as well as the experimental results by Whan & Rothfus (1959) and Patel & Head (1969), are also presented in figure 2. It is clear that the values of the drag coefficient C_f in all two-dimensional secondary flows differ substantially from the experimental data. In contrast, the drag coefficients in the computed three-dimensional secondary flows agree rather well with experimental data on turbulent flows.

A few two-dimensional secondary flows were computed several times, with an increased spatial–temporal resolution and with alteration of the numerical technique. The purpose of these calculations was to confirm the stability of secondary flows to inaccuracies in their numerical simulation. Changes in secondary flows proved to be insignificant.

In §2 we present the mathematical formulation of the problem, as well as one version of our numerical technique. In §3 the basic results on two-dimensional secondary flows are presented. Results on three-dimensional secondary flows are described and compared with experiments in §4. The present results are discussed and compared with those obtained by other authors in §5.

2. Mathematical formulation of the problem and numerical technique

The problem of a periodic incompressible viscous fluid flow in a plane infinite channel $K \equiv [\boldsymbol{X} = \{x, y, z\}: |x|, |y| < \infty; |z| \leqslant 1]$ can be reduced to determining the solution of the Navier–Stokes equations

$$\frac{\partial \boldsymbol{V}(\boldsymbol{X},t)}{\partial t} + (\boldsymbol{V}(\boldsymbol{X},t), \boldsymbol{\nabla})\, \boldsymbol{V}(\boldsymbol{X},t) = -\boldsymbol{\nabla} p(\boldsymbol{X},t) + \nu \nabla^2 \boldsymbol{V}(\boldsymbol{X},t), \tag{2.1}$$

$$\boldsymbol{\nabla} \cdot \boldsymbol{V}(\boldsymbol{X},t) = 0 \tag{2.2}$$

that satisfies the no-slip condition on the channel walls $z = \pm 1$:

$$\boldsymbol{V}(x, y, z = \pm 1, t) = 0 \tag{2.3}$$

and the periodicity conditions with respect to the x-, y-variables:

$$\boldsymbol{V}(x, y, z, t) = \boldsymbol{V}(x + X, y, z, t) = \boldsymbol{V}(x, y + Y, z, t). \tag{2.4}$$

Here ν is the kinematic viscosity coefficient, $\boldsymbol{V}(\boldsymbol{X},t) = \{u(\boldsymbol{X},t), v(\boldsymbol{X},t), w(\boldsymbol{X},t)\}$ is the velocity field of the flow, $p(\boldsymbol{X},t)$ is the pressure (the density of the fluid is assumed to be constant, $\rho_0 \equiv 1$).

In our method of the numerical solution of the problem (2.1)–(2.4) the solution is represented in the form

$$\boldsymbol{V}(\boldsymbol{X},t) = \boldsymbol{U}_0(z) + \boldsymbol{V}'(\boldsymbol{X},t), \tag{2.5}$$

$$p(\boldsymbol{X},t) = -2\nu x + p'(\boldsymbol{X},t), \tag{2.6}$$

where $\boldsymbol{U}_0(z) = \{U_0(z) = 1 - z^2, 0, 0\}$ (in what follows the primes on the velocity and pressure deviations from their values for the Poiseuille flow are omitted). Upon substituting (2.5) and (2.6) into (2.1)–(2.4) we obtain

$$\frac{\partial \boldsymbol{V}(\boldsymbol{X},t)}{\partial t} = [\boldsymbol{V}(\boldsymbol{X},t), \boldsymbol{\omega}(\boldsymbol{X},t)] - \mathbf{L}[\boldsymbol{V}(\boldsymbol{X},t)] - \boldsymbol{\nabla} \Pi(\boldsymbol{X},t) + \nu \nabla^2 \boldsymbol{V}(\boldsymbol{X},t), \tag{2.7}$$

$$\boldsymbol{\nabla} \cdot \boldsymbol{V}(\boldsymbol{X},t) = 0, \tag{2.8}$$

$$V(x, y, z = \pm 1, t) = 0, \tag{2.9}$$

$$V(x, y, z, t) = V(x+X, y, z, t) = V(x, y+Y, z, t), \tag{2.10}$$

$$\Pi(x, y, z, t) = \Pi(x+X, y, z, t) = \Pi(x, y+Y, z, t), \tag{2.11}$$

where

$$\omega(\boldsymbol{X}, t) = [\nabla, \boldsymbol{V}(\boldsymbol{X}, t)], \quad \Pi(\boldsymbol{X}, t) = p(\boldsymbol{X}, t) + \tfrac{1}{2}\boldsymbol{V}^2(\boldsymbol{X}, t),$$

and the linear operator $\mathbf{L}[\boldsymbol{V}(\boldsymbol{X}, t)]$ is given by the formula

$$\mathbf{L}[\boldsymbol{V}(\boldsymbol{X}, t)] = \left\{U_0(z)\frac{\partial u}{\partial x} + U_0'(z)\, w,\ U_0(z)\frac{\partial v}{\partial x},\ U_0(z)\frac{\partial w}{\partial x}\right\}.$$

The conditions (2.11) in combination with (2.6) mean that the space-averaged pressure gradient equal to $-2\nu \boldsymbol{i}$, $\boldsymbol{i} = \{1, 0, 0\}$, is fixed. Therefore the Reynolds number $R_p = 1/\nu$ is ascribed to all the flows studied here.

The approximate solution of the problem (2.7)–(2.11) is searched for in the form

$$\begin{Bmatrix} \boldsymbol{V}(\boldsymbol{X}, t) \\ \Pi(\boldsymbol{X}, t) \end{Bmatrix} = \sum_{|m| \leqslant M} \sum_{|n| \leqslant N} \sum_{p=0}^{P} \begin{Bmatrix} \boldsymbol{V}_{mnp}(t) \\ \Pi_{mnp}(t) \end{Bmatrix} T_p(z) \exp[im\alpha_0 x + in\beta_0 y], \tag{2.12}$$

where $\alpha_0 = 2\pi/X$, $\beta_0 = 2\pi/Y$, $T_p(z) = \cos(p \arccos z)$ are Chebyshev polynomials. In order that the solution be real-valued the following conditions should be satisfied:

$$\boldsymbol{V}^*_{m,n,p}(t) = \boldsymbol{V}_{-m,-n,p}(t), \quad \Pi^*_{m,n,p}(t) = \Pi_{-m,-n,p}(t),$$

where the asterisk refers to complex-conjugate quantities. Note that Chebyshev polynomials in numerical calculations of such a problem were used by Herbert (1977), Orszag & Kells (1980), Moin & Kim (1980) and others.

The integration in time of the problem (2.7)–(2.11) is carried out by the fractional step method (see Yanenko 1967; Samarsky 1977).

Three fractional steps are introduced. At the first fractional step in the mixed spectral–physical representation (for the x-, y-variables – in the space of Fourier coefficients, and for z – in the physical space at the mesh nodes $z_l = \cos(\pi l/P)$, $l = 0, 1, \ldots, P$) the solution of the explicit difference scheme

$$\frac{\boldsymbol{V}^{k+\frac{1}{3}}_{mnl} - \boldsymbol{V}^k_{mnl}}{\tau} = \tfrac{3}{2}\boldsymbol{F}^k_{mnl} - \tfrac{1}{2}\boldsymbol{F}^{k-1}_{mnl} - \tfrac{1}{2}im\alpha_0 U_l \boldsymbol{V}^k_{mnl} - iU_l'(\tfrac{5}{2}w^k_{mnl} - w^{k-1}_{mnl}) \tag{2.13}$$

is determined, where $\boldsymbol{i} = \{1, 0, 0\}$, $\boldsymbol{F} = [\boldsymbol{V}, \boldsymbol{\omega}]$, U_l and U_l' are the values of $U_0(z)$ and its derivative at the point z_l. The pseudospectral method of calculation of the nonlinear terms (see Orszag 1971) is applied.

At the second fractional step the solution of the following purely implicit difference scheme is determined:

$$\frac{\boldsymbol{V}^{k+\frac{2}{3}}(\boldsymbol{X}) - \boldsymbol{V}^{k+\frac{1}{3}}(\boldsymbol{X})}{\tau} = -\nabla \Pi^{k+\frac{2}{3}}(\boldsymbol{X}) + \nu\nabla^2 \boldsymbol{V}^{k+\frac{2}{3}}(\boldsymbol{X}), \tag{2.14}$$

$$\nabla \cdot \boldsymbol{V}^{k+\frac{2}{3}}(\boldsymbol{X}) = 0, \tag{2.15}$$

$$\boldsymbol{V}^{k+\frac{2}{3}}(x, y, z = \pm 1) = 0. \tag{2.16}$$

The problem (2.14)–(2.16) is effectively solved in a representation spectral in all spatial variables. In the z-variable the method of Petrov (1940) is employed. This method is also called the spectral tau-method (Lanczos 1956; Fox 1962).

In our algorithms the components of $\boldsymbol{V}^{k+\frac{2}{3}}$ are computed consecutively.

At first the systems of linear equations

$$\left.\begin{gathered} -\gamma_{mn}^2(1+\tau\nu\gamma_{mn}^2)\,w_{mnp}^{k+\frac{2}{3}}+(1+2\tau\nu\gamma_{mn}^2)\,w_{mnp}^{(2)k+\frac{2}{3}}-\tau\nu w_{mnp}^{(4)k+\frac{2}{3}}=f_{mnp}, \\ p=0,1,\ldots,P-4, \\ \sum_{p=0}^{P} w_{mnp}^{k+\frac{2}{3}}=\sum_{p=0}^{P}(-1)^p\,w_{mnp}^{k+\frac{2}{3}}=\sum_{p=0}^{P-1} w_{mnp}^{(1)k+\frac{2}{3}}=\sum_{p=0}^{P-1}(-1)^p\,w_{mnp}^{(1)k+\frac{2}{3}}=0, \end{gathered}\right\} \tag{2.17}$$

are solved, where $|m|\leqslant M$, $|n|\leqslant N$, $\gamma_{mn}^2=\alpha_0^2m^2+\beta_0^2n^2>0$,

$$f_{mnp}=-\gamma_{mn}^2\,w_{mnp}^{k+\frac{1}{3}}-\mathrm{i}\alpha_0 m u_{mnp}^{(1)k+\frac{1}{3}}-\mathrm{i}\beta_0 n v_{mnp}^{(1)k+\frac{1}{3}}.$$

As a result the expansion coefficients $w_{mnp}^{k+\frac{2}{3}}$ of the z-component of velocity are obtained.

The values $a_p^{(1)}$, $a_p^{(2)}$ and $a_p^{(4)}$ in (2.17) are computed by the formulae:

$$a_p^{(1)}=\frac{2}{C_p}\sum_{s=p+1,\ s+p\equiv 1(\mathrm{mod}\,2)}^{P} s a_s \quad (p=0,1,\ldots,P-1), \tag{2.18}$$

$$a_p^{(2)}=\frac{1}{C_p}\sum_{s=p+2,\ s\equiv p(\mathrm{mod}\,2)}^{P} s(s^2-p^2)\,a_s \quad (p=0,1,\ldots,P-2), \tag{2.19}$$

$$a_p^{(4)}=\frac{1}{24C_p}\sum_{s=p+4,\ s\equiv p(\mathrm{mod}\,2)}^{P} s[s^2(s^2-4)^2-3p^2s^4+3p^4s^2-p^2(p^2-4)^2]\,a_s \quad (p=0,1,\ldots,P-4), \tag{2.20}$$

where $C_0=2$, $C_p=1$ for $p\geqslant 1$; $s\equiv p\,(\mathrm{mod}\,2)$ means that $s-p$ is even. The systems (2.17) are solved with a high accuracy by means of a well-designed rapid technique (see Rozhdestvensky & Simakin 1982*a*). After $w_{mnp}^{k+\frac{2}{3}}$ are known, two other velocity components may be easily found.

It should be emphasized that the spectral tau-method possesses a high accuracy. However, in some cases the application of this method results in spurious roots, which make the spatial approximation of the evolution differential problem absolutely unstable (see e.g. Rozhdestvensky, Ermakova & Priymak 1977; Rozhdestvensky & Yanenko 1978; Gottlieb & Orszag 1977). In the case of the purely implicit difference scheme (2.17), this shortcoming is manifested in a quite original manner: the scheme becomes conditionally stable with the limitation of the time step τ from below, $\tau>\tau_0\sim 2/(\nu P^4)\to 0$ as $P\to\infty$. In our calculations $R_p=1/\nu\leqslant 12000$ and $P\geqslant 32$, consequently $\tau_0\lesssim 0.02$. At the same time the considered scheme at $\tau=0.1, 0.05$ possesses a high reliability and accuracy.

At the final third fractional step in the mixed spectral–physical representation (as at the first fractional step) the solution of the implicit difference scheme

$$\frac{V_{mnl}^{k+1}-V_{mnl}^{k+\frac{2}{3}}}{\tau}=-\tfrac{1}{2}\mathrm{i}m\alpha_0\,U_l\,V_{mnl}^{k+1}+\boldsymbol{i}\tfrac{1}{2}U_l'w_{mnl}^{k+1} \tag{2.21}$$

is obtained. Step (2.21) symmetrizes the first fractional step and improves the approximation of the linear term $\mathbf{L}[\boldsymbol{V}(\boldsymbol{X},t)]$. The third fractional step completes the calculation of the full step, and we have the vector $\boldsymbol{V}^{k+1}(\boldsymbol{X})$ as the initial condition for the next time step.

It is not difficult to show that the solution $\boldsymbol{V}^{k+1}(\boldsymbol{X})$ satisfies the incompressibility condition (2.8) and the no-slip condition (2.9).

Note that the calculations of the nonlinear term $\boldsymbol{F}=[\boldsymbol{V},\boldsymbol{\omega}]$ and the transitions in the z-variable from physical to Fourier space and conversely are performed by means of the new algorithm of fast Fourier transform by Kaporin (1980).

Concluding here the brief presentation of our numerical technique, we refer the reader for further details to Rozhdestvensky & Simakin (1982*a*) and Simakin (1983*a*).

Note that we have also constructed an analogous scheme for the other formulation of the problem (at fixed flow rate).

We have carried out a detailed spectral analysis of the stability and accuracy of these numerical schemes in a wide range of the wavenumbers for subcritical and supercritical Reynolds numbers. A description of the spectral analysis as a method of investigation of the stability and accuracy of numerical algorithms for solution of the Navier–Stokes equations was given by Rozhdestvensky (1973).

This method enables us to determine both the maximal allowable integration time step and the necessary accuracy of the spatial approximation which will assure an acceptable accuracy of the computational algorithm when applied to the description of the linear evolution of disturbances.

It was found that for a comparatively small number of basis functions and for a rather large time step $\tau = 0.1$ our schemes are stable and have an acceptable approximation accuracy both in space and time.

In addition, it was found that the 'excessive' eigenvalues due to the three-time-level character of the schemes have a considerable negative real part as compared with the larger true eigenvalues. Consequently the disturbances corresponding to 'excessive' roots decay rapidly, and influence the solution insignificantly.

Note also, that at $P \gtrsim 30$–40 and $\tau \sim 0.1$ the constructed schemes are stable in a wide range of wavenumbers α and β. This was achieved by the use of a semi-implicit treatment of the linear term $\mathbf{L}[V]$ in our schemes.

By means of the spectral analysis of the numerical schemes we were able to evaluate the action of the individual terms of the Navier–Stokes equations and to find the optimal parameters for our schemes. This enables us to perform a large number of computations of two- and three-dimensional flows over considerable intervals of time by use of computers of moderate capacity.

More detailed presentation of the results of the spectral analysis of ours and some other schemes is given in Simakin (1983*a*).

3. Two-dimensional secondary flows

By means of our method presented in §2 as well as some of its modifications a search for two-dimensional secondary flows was carried out in the R_p range from 2000 to 12000.

Imposing a certain velocity field $V_0(X)$ (which differs from the velocity in Poiseuille flow, and which satisfies $\nabla \cdot V_0 = 0$) as the initial velocity at $t = 0$ we compute the evolution of corresponding flow until R_Q became steady, i.e. the flow became a secondary or Poiseuille flow. The mean time of the passage of the flow to a secondary regime was $T = O(1/\nu)$.

The passage of the flow to a secondary flow was controlled by the stabilization of its principal integral characteristics such as the flow rate Q, and total energy of disturbances. At the final stage of all our computations of two-dimensional secondary flows the flow rate is practically constant: its variation does not exceed 0.1% of its value.

In the first series of runs the evolution of finite disturbances with periodicity intervals $X \lesssim 2\pi$ ($\alpha_0 \gtrsim 1$) was computed (short-wavelength disturbances). Three runs were performed at $R_p = 2935$ and $\alpha_0 = 1.3231$ (see table 1, runs 1–3). As the initial

Run	Reynolds number R_p	Minimal wave-number α_0	Number of basis functions $(2M+1)(P+1)$	Time step τ	Termination time of computation $T\times10^{-2}$	Reynolds number R_Q	Normal-ized flow rate Q/Q_0	Total energy of disturb-ances $E\times10$
1	2935	1.3231	9×33	0.1	10	2935	1	0
2	2935	1.3231	17×33	0.05	30	2935	1	0
3	2935	1.3231	9×33	0.05	30	2935	1	0
4	2935	0.9923	17×33	0.05	10	2935	1	0
5	5000	1.25	9×33	0.05	60	3616	0.723	0.533
6	4500	1.25	9×33	0.05	55	3413	0.758	0.421
7	4000	1.25	9×33	0.05	45	3183	0.796	0.318
8	3500	1.25	9×33	0.05	40	2952	0.843	0.204
9*	3250	1.25	9×33	0.05	35	2855	0.879	0.132
10	3000	1.25	9×33	0.05	35	3000	1	0
11*	4000	1.3	9×33	0.05	45	3130	0.783	0.346
12*	5000	1.35	9×33	0.05	55	3376	0.675	0.689
13	5000	1.5	9×33	0.05	45	5000	1	0
14	6250	1.25	9×33	0.05	70	4165	0.666	0.736
15*	6250	1.5	9×33	0.05	70	3806	0.609	0.963
16	7500	1.25	9×33	0.05	80	4671	0.623	0.913
17*	7500	1.5	9×33	0.05	80	4216	0.562	1.184
18	7500	1.7	9×33	0.05	70	7500	1	0
19	8750	1.25	9×65	0.05	90	5159	0.590	1.060
20	8750	1.5	9×65	0.05	90	4620	0.528	1.356
21	10000	1.0	9×65	0.05	110	6945	0.695	0.605
22	10000	1.25	9×65	0.05	100	5605	0.561	1.196
23	10000	1.5	9×65	0.05	90	5022	0.502	1.495
24*	10000	1.65	9×65	0.05	90	4914	0.491	1.540
25	10000	1.7	9×65	0.05	60	10000	1	0
26	12000	1.25	9×65	0.05	120	6239	0.520	1.385
27	12000	1.5	9×65	0.05	100	5564	0.464	1.698
28*	12000	1.65	9×65	0.05	110	5442	0.454	1.759
29	12000	1.75	9×65	0.05	70	12000	1	0

TABLE 1. Characteristics of the two-dimensional computations of the evolution of short-wavelength finite-amplitude disturbances in plane Poiseuille flow (asterisks indicate the limit secondary flows)

disturbance the first Fourier mode $V_{m=1}(z) = \{u_1(z), 0, w_1(z)\}$ was given with different energies

$$E_1(0) = \frac{1}{2}\int_{-1}^{1} \{|u_1(z)| + |w_1(z)|^2\}\,dz = 2.16\times10^{-3},\ 5.11\times10^{-3},\ 2.973\times10^{-2}.$$

Here $V_1(z)$ is the eigenfunction of the linearized scheme (2.13)–(2.21) corresponding to the senior eigenvalue. Having performed runs 1–3 over considerable intervals of time, we made certain that the disturbances completely decayed when $t\to\infty$, since in the end of runs 1–3 the disturbances were decaying in accordance with the linear theory.

Imposing an initial disturbance similarly to foregoing runs (the energy $E_1(0) = 1.56\times10^{-2}$) we succeeded in obtaining a two-dimensional secondary flow at the Reynolds number $R_p = 5000$ and $\alpha_0 = 1.25$ (see run 5, table 1). This flow passed

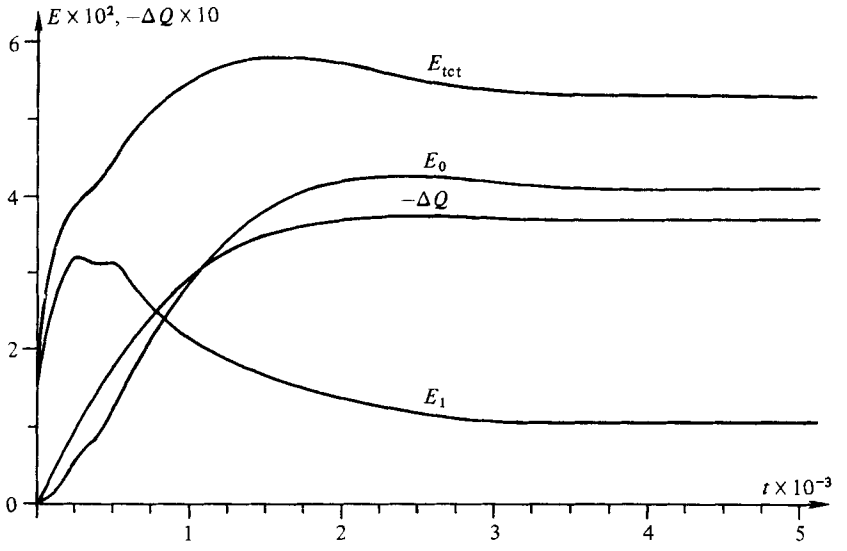

FIGURE 3. Evolution of the total energy of disturbances, decrease of the flow rate, and energies of the zeroth and first harmonics in the two-dimensional run 5 ($R_p = 5000$, $\alpha_0 = 1.25$).

to the secondary regime with with the constant $R_Q = 3616$. In figure 3 we present the evolution of the flow-rate change

$$\Delta Q(t) = \int_{-1}^{1} u_0(z,t)\,\mathrm{d}z$$

of the total energy of disturbances per unit length

$$E_{\mathrm{tot}}(t) = \frac{1}{2X}\int_0^X \int_{-1}^{1} [u^2(x,z,t) + w^2(x,z,t)]\,\mathrm{d}x\,\mathrm{d}z,$$

and the energies of harmonics

$$E_m(t) = \frac{1}{2}\int_{-1}^{1} [|u_m(z,t)|^2 + |w_m(z,t)|^2]\,\mathrm{d}z,$$

for $m = 0, 1$ in run 5.

In table 1 for the time corresponding to termination of the computations the values of basic characteristics of secondary flows are presented: the Reynolds number R_Q, the flow rate normalized by its value for Poiseuille flow, and the total energy of disturbances per unit length.

Taking as a basis the secondary flow obtained at $R_p = 5000$ and $\alpha_0 = 1.25$, we were able to go over gradually to smaller values of Reynolds numbers R_p and other values of α_0. This search technique noticeably reduces the time of passage of the flow to the secondary regime.

The next run was performed at $R_p = 4500$ and $\alpha_0 = 1.25$. As the initial condition the velocity field was set which was obtained in the previous run at $t = 5000$. In this run a secondary flow with constant $R_Q = 3413$ was obtained (see table 1, run 6).

Acting in a similar way we found secondary flows at $R_p = 4000, 3250$ and $\alpha_0 = 1.25$.

For $R_p < 3250$ and $\alpha_0 = 1.25$ we failed in finding two-dimensional secondary flows.

Farther in the range of $R_p = 3250$–12000 the search for secondary flows was carried out for various $\alpha_0 \gtrsim 1$. After a large number of computations we obtained several

Run	Reynolds number R_p	Minimal wave-number α_0	Number of basis functions $(2M+1)(P+1)$	Time step τ	Termination time of computation $T\times10^{-2}$	Reynolds number R_Q	Normal-ized flow rate Q/Q_0	Total energy of disturb-ances $E\times10^2$
30	2935	0.3387	33×33	0.05	70	2723	0.928	0.615
31	2900	0.3387	33×33	0.05	60	2701	0.931	0.568
32	2850	0.3387	33×33	0.05	50	2672	0.937	0.501
33	2800	0.33	33×33	0.05	50	2642	0.944	0.431
34	2750	0.33	33×33	0.05	40	2612	0.950	0.386
35	2700	0.33	33×33	0.05	30	2700	1	0
36	2700	0.15	33×33	0.05	35	2700	1	0
37	3500	0.3	33×33	0.05	60	2957	0.845	2.003
38	4800	0.3	33×33	0.05	70	3578	0.746	4.586
39	6250	0.3	33×33	0.05	80	4275	0.684	6.639
40	7500	0.3	33×33	0.05	95	4818	0.642	8.217
41	8750	0.3	33×33	0.05	95	5361	0.613	9.443
42	12000	0.15	33×33	0.05	130	5718	0.477	16.299

TABLE 2. Characteristics of the two-dimensional computations of the evolution of long-wavelength finite-amplitude disturbances in plane Poiseuille flow

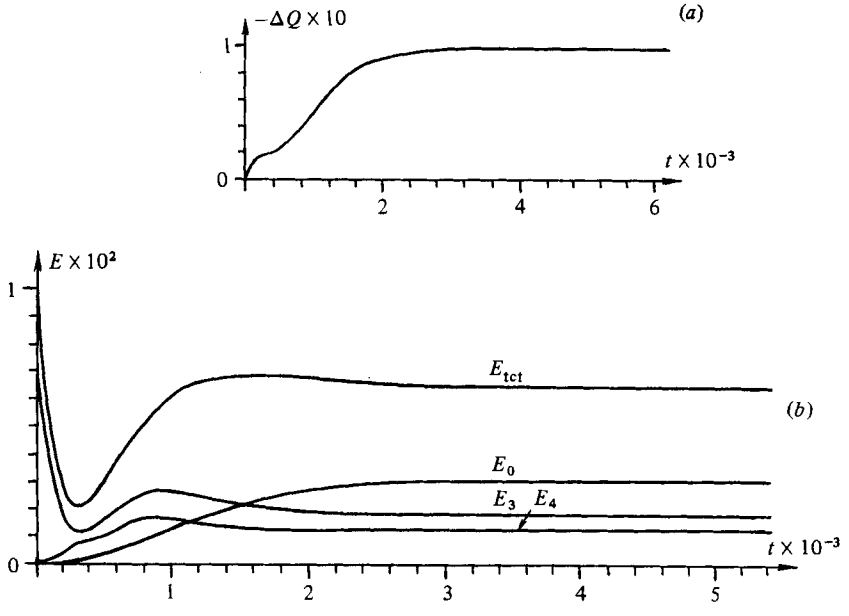

FIGURE 4. (*a*) Decrease of the flow rate with time t in run 30 ($R_p = 2935$, $\alpha_0 = 0.3387$). (*b*) Total energy of disturbances, energies of the zeroth, third and fourth harmonics versus time t in run 30.

classes of secondary flows (see table 1). It was discovered that for any $R_p \geqslant 3250$ there exist a set of two-dimensional secondary flows with different periodicity intervals $X \lesssim 2\pi$ (see figure 1). Among them there exists the 'limiting' flow in which the minimal flow rate (at fixed R_p) and the maximal drag (at fixed R_Q) are realized. For some Reynolds numbers $R_p \in [3250, 12000]$ secondary flows were obtained which are

sufficiently close to the 'limiting' flows. In table 1 such flows are marked by an asterisk.

In the next series of runs a search for two-dimensional secondary flows with different periodicity intervals $X \gtrsim 6\pi$ was undertaken.

Run 30 (see table 2) was performed at $R_p = 2935$ and $\alpha_0 = 0.3387$. As the initial disturbance the first five Fourier modes were imposed in the representation of the approximate solution (2.12) with different energies $E_1(0) = E_2(0) = 1.30 \times 10^{-3}$, $E_3(0) = 6.81 \times 10^{-3}$, $E_4(0) = E_5(0) = 8.24 \times 10^{-5}$. In figure 4 (*a*) the change $\Delta Q(t)$ in the flow rate is plotted. It is seen that at the beginning the flow rate decreases, and when $t \gtrsim 3200$ it becomes practically constant. Similar passage to the constants of the total energy of disturbance $E_{\text{tot}}(t)$ and the energies of harmonics $E_m(t)$, $m = 0, 3, 4$, is observed (see figure 4*b*). Note that among the harmonics that are taken into account in the representations (2.12) those corresponding to $m = 0, 3, 4$ have the greatest energies.

In the next runs at $R_p = 2000$–2800 and $\alpha_0 = 0.15$ to 0.3387 we did not succeed in finding secondary flow when imposing the initial condition in a way similar to the previous run 30. However, taking the velocity field of the secondary flow obtained in run 30 as the initial condition, we computed the secondary flow at $R_p = 2900$ and $\alpha_0 = 0.3387$. Decreasing the Reynolds number R_p in such a way, we found secondary flows up to $R_p = 2750$ ($R_Q = 2612$).

The basic integral characteristics of these flows are presented in table 2.

A few computations of the long-wavelength disturbance evolution were performed for larger Reynolds numbers. Two-dimensional secondary flows with periodicity interval $X = 2\pi/0.3$ for $R_p = 3500$–8750 and at $R_p = 12000$, $X = 2\pi/0.15$ were obtained (see table 2).

Thus for $R_p \in [2750, 3000]$ the two-dimensional secondary flows were found only for $\alpha_0 \lesssim 0.3$. This means the instability of Poiseuille flow to finite-amplitude long-wavelength disturbances when $R_p \gtrsim 2750$ ($R_Q \gtrsim 2612$).

Some runs were performed with the goal of evaluating the influence of initial conditions over the integral characteristics of a secondary flow. In three runs at $R_p = 3500$ and $\alpha_0 = 0.3$ different initial conditions were imposed. In these runs the secondary flows were obtained for which the flow rates as well as the total energies of disturbances just coincided (see figures 5*a*, *b*). Analogous results were obtained in computations at $R_p = 3500$, $\alpha_0 = 1.25$ and $R_p = 7500$, $\alpha_0 = 0.3$ with various initial conditions.

Thus these computations confirm the fact that the values of integral characteristics of two-dimensional secondary flows do not depend upon the initial conditions, but are determined only by the Reynolds number and the interval of periodicity.

The results of each run can be recalculated for the other external condition ($Q = \text{const}$), since in each secondary flow the flow rate $Q(t)$ is practically constant. The deviations of the mean-velocity profile of the secondary flow from the profile in the Poiseuille flow with the same flow rate (that is at $R = R_Q$) are calculated by the formula

$$\langle V'_Q(x, z, t)\rangle_x = \frac{|\Delta Q|}{Q_0}(1 - z^2) + \langle V'_p(x, z, t)\rangle_x, \tag{3.1}$$

where $|\Delta Q|$ is the reduction of the flow rate, $Q_0 = \frac{4}{3}$ is the flow rate for Poiseuille flow and $\langle V'_Q(x, z, t)\rangle_x$, $\langle V'_p(x, z, t)\rangle_x$ are mean profiles of the velocity disturbance in the problem with the fixed flow rate and the fixed mean-pressure gradient respectively.

The mean-velocity disturbance profile $\langle V'_p(x, z, t)\rangle_x$ obtained in run 30

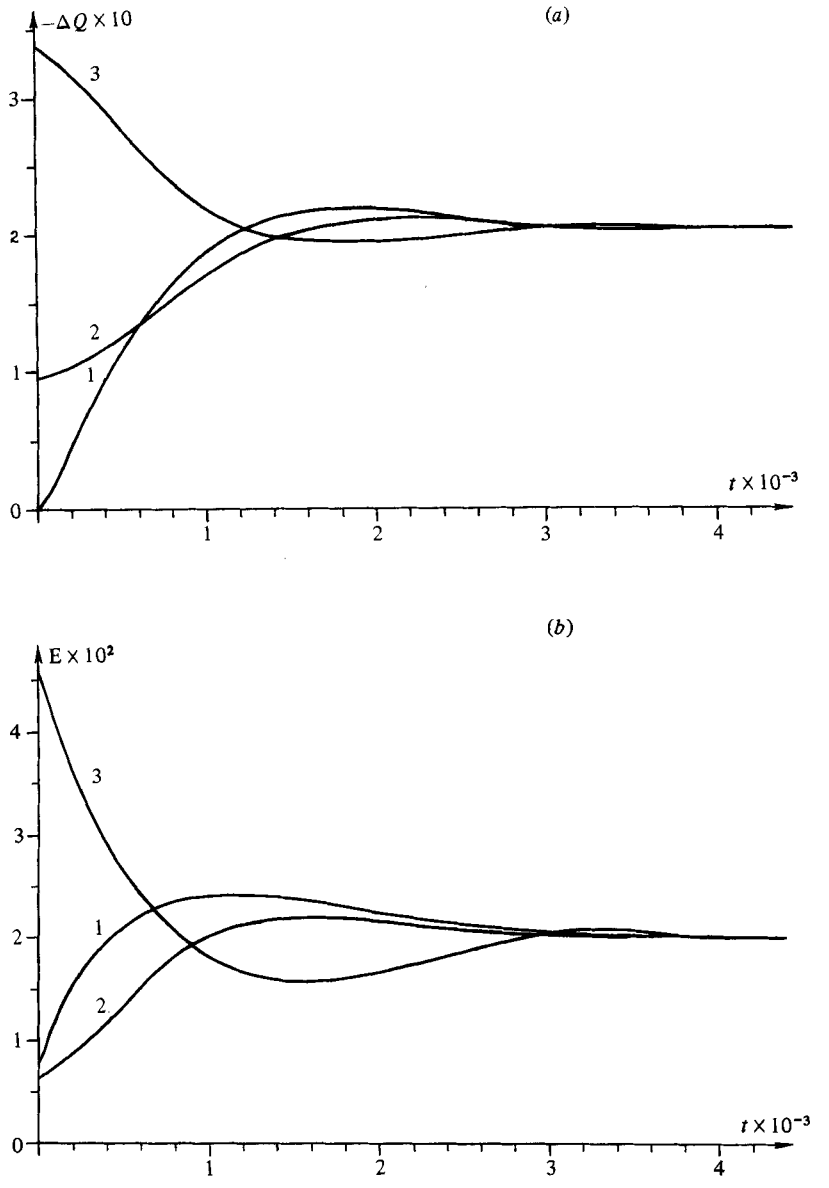

FIGURE 5. Study of the influence of initial conditions. (*a*) Decrease of flow rate at $R_p = 3500$, $\alpha_0 = 0.3$ with time. (*b*) Same as (*a*), but for total energy of disturbances.

($R_p = 2935$, $\alpha_0 = 0.3387$) at $t = 5005$, 5010, 5015 as well as the result of its recalculation $\langle V'_Q(x,z,t)\rangle_x$ ($R_Q = 2723$) are presented in figure 6. We see that at $R_Q = 2723$ the averaged profile $\langle V'_Q(x,z,t)\rangle_x$ has three positive maxima: two near the walls and one at the centre. Note that similar forms of averaged velocity disturbance profiles were obtained by Shkadov (1973*b*), Zahn *et al.* (1974) and Rozhdestvensky & Priymak (1982).

The same graphs but for run 42 ($R_p = 12000$, $R_Q = 5718$, $\alpha_0 = 0.15$) at $t = 8000$ are plotted in figure 7. It is seen that a positive maximum in the mean profile $\langle V'_Q\rangle_x$ at the centre of the channel vanishes as R_Q increases.

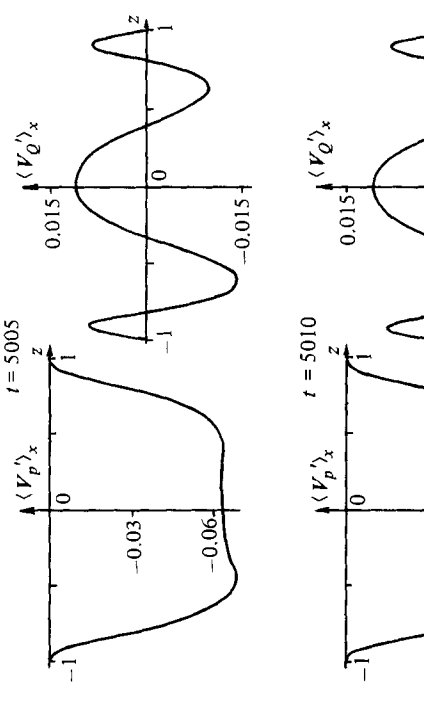

FIGURE 6. Mean-disturbance-velocity profiles in the two-dimensional secondary flow $R_p = 2935$, $\alpha_0 = 0.3387$ (run 30) and results of their recalculations for the problem with a fixed flux ($R_Q = 2723$).

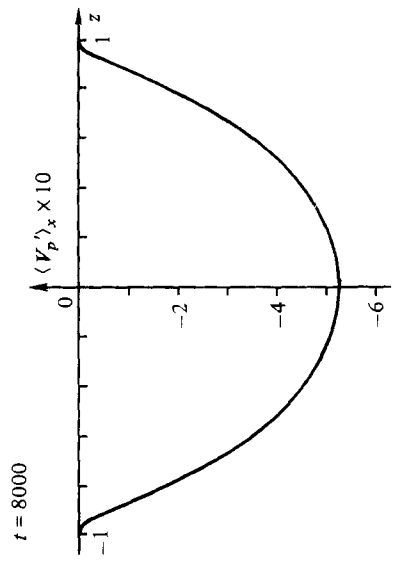

FIGURE 7. Same as in figure 6, but for secondary flow $R_p = 12000$, $R_Q = 5718$, $\alpha_0 = 0.15$ (run 42).

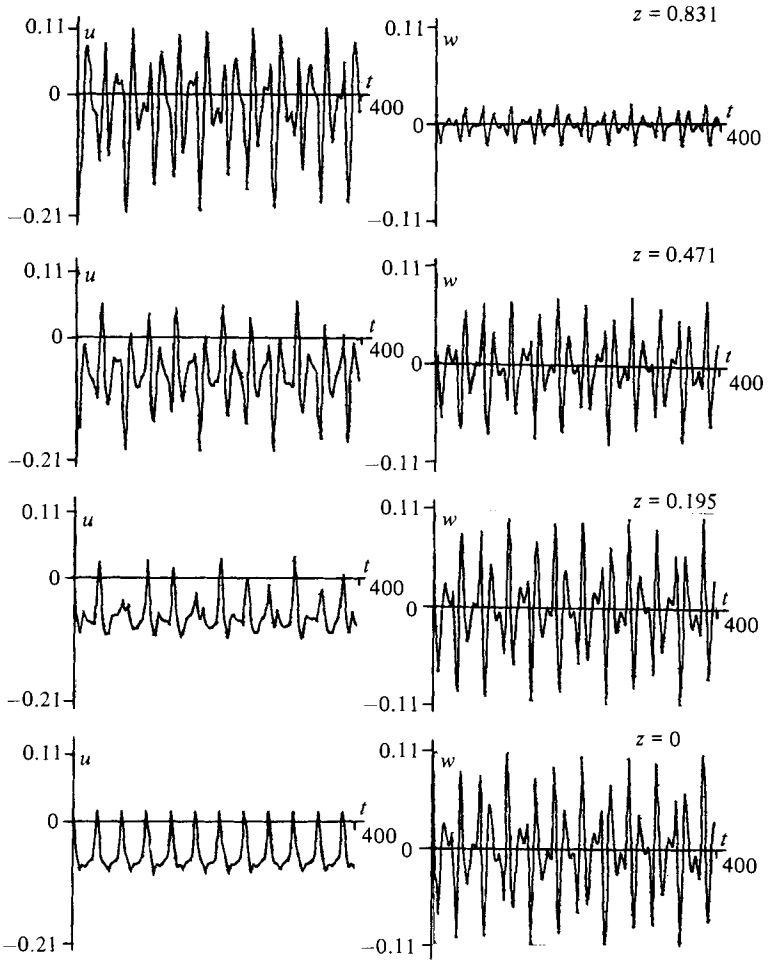

FIGURE 8. Behaviour of the longitudinal u- and transverse w-components of the velocity of disturbances over the time interval $t = 5000$–5400 at different points $\{x = 0, z_k\}$, $R_p = 2935$, $\alpha_0 = 0.3387$ (run 30).

In figure 8 the evolution of longitudinal $u(x, z, t)$ and transverse $w(x, z, t)$ components of the velocity of disturbances ($R_p = 2935$, $\alpha_0 = 0.3387$, run 30) in the time interval $(5000, 5400)$ is given at the following points of the channel: $\{x, z_k\} = \{x = 0; z_1 = 0.831, z_2 = 0.471, z_3 = 0.195, z_4 = 0\}$. It is seen that the amplitude of oscillations of $u(x, z, t)$ is maximal near the channel walls. For the transverse component $w(x, z, t)$ the picture is converse: the level of fluctuations increases on approaching the channel centre.

In figure 9(a) we plot instantaneous level lines of the function $\psi(x, z, t)$, where $\partial\psi/\partial z = u$, $\partial\psi/\partial x = -w$ for the two-dimensional secondary flow at $R_p = 2935$ and $\alpha_0 = 0.3387$ (run 30). Note that $V = \{u, 0, w\}$ is the deviation of the flow velocity from the velocity in the Poiseuille flow at $R = R_p$ (see §2). In figure 9(b) instantaneous streamlines for the secondary flow at $R_p = 12000$ and $\alpha_0 = 0.15$ (run 42) are presented. In contrast with figure 9(a), the streamlines of the flow are calculated by the total velocity: $\partial\psi/\partial z = U_0(z) + u$, $\partial\psi/\partial x = -w$. An intermittence phenomenon characteristic of turbulent flows is observed: the regions of strongly pulsating flow (region A) are separated by a region of less-pulsating flow (region B). Note that the dimensions of the eddies decrease with increase in the Reynolds number.

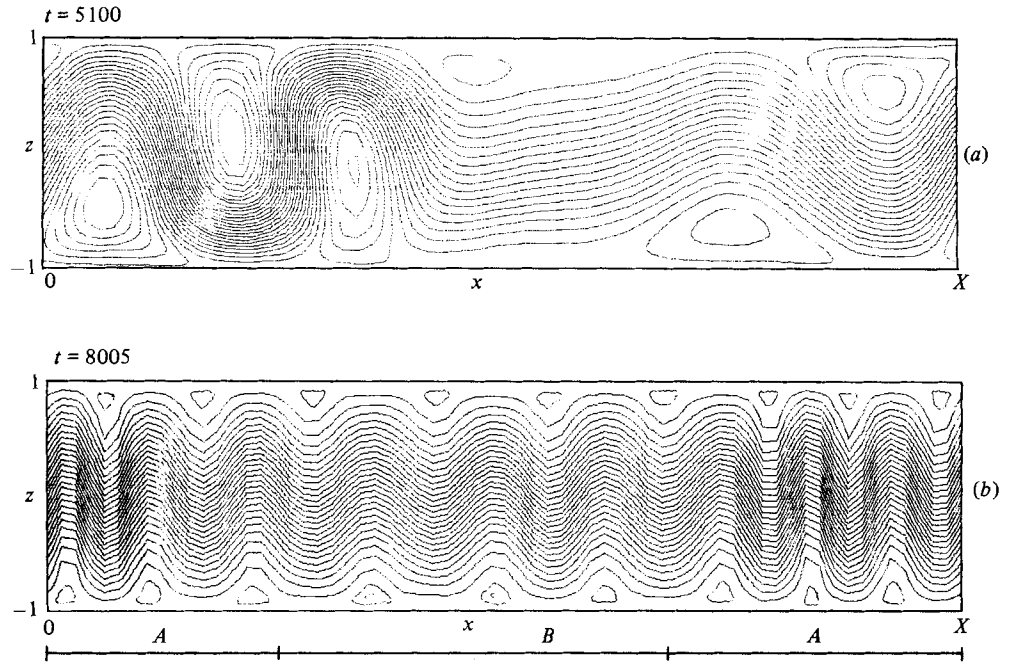

FIGURE 9. (*a*) Instantaneous pictures of the level curves of the function $\psi(x, z, t)$, where $\partial\psi/\partial z = u$, $\partial\psi/\partial x = -w$ for two-dimensional secondary flow at $R_p = 2935$, $\alpha_0 = 0.3387$ (run 30). Note that the full velocity of the flow is $V = \{u + U_0(z), 0, w\}$. (*b*) Instantaneous picture of the level curves of the stream function for two-dimensional secondary flow at $R_p = 12000$, $\alpha_0 = 0.15$ (run 42). The regions of strongly pulsating flow (regions A) are separated by a region of a less-pulsating flow (region B).

The long-wavelength secondary flows are rather unusual objects in the theory of hydrodynamical stability; in particular, they are non-periodic in time. For this reason we have investigated the temporal behaviour of the coefficients of the velocity-field expansion of the two-dimensional secondary flow (2.12) at $R_p = 2935$ and $\alpha_0 = 0.3387$. It turned out that the dependencies of coefficients $u_{mp}(t)$ and $w_{mp}(t)$ were close to the following:

$$\left.\begin{aligned} u_{0,\,2s}(t) &= A_{0,\,2s}, \\ u_{0,\,2r+1}(t) &= A_{0,\,2r+1}\exp(-\mathrm{i}\omega_0 t); \end{aligned}\right\} \tag{3.2}$$

$$\left.\begin{aligned} u_{m,\,2s}(t) &= A_{m,\,2s}\exp(-\mathrm{i}\omega_m t), \\ w_{m,\,2r+1}(t) &= B_{m,\,2r+1}\exp(-\mathrm{i}\omega_m t) \end{aligned}\right\} \quad (m \neq 0); \tag{3.3}$$

$$\left.\begin{aligned} u_{m,\,2r+1}(t) &= A_{m,\,2r+1}\exp(-\mathrm{i}\bar{\omega}_m t), \\ w_{m,\,2s}(t) &= B_{m,\,2s}\exp(-\mathrm{i}\bar{\omega}_m t) \end{aligned}\right\} \quad (m \neq 0); \tag{3.4}$$

where $|m| \leqslant M$, $s = 0, \ldots, \frac{1}{2}P$, $r = 0, \ldots, \frac{1}{2}P - 1$; A_{mp} and B_{mp} are constant.

Substituting the representations (3.2)–(3.4) into the expansion (2.12), we get

$$\left.\begin{aligned} u(x,z,t) &= u_0(z) + \bar{u}_0(z)\cos(\omega_0 t) + \sum_{m=1}^{M}[u_m(x - C_m t, z) + \bar{u}_m(x - \bar{C}_m t, z)], \\ w(x,z,t) &= \sum_{m=1}^{M}[w_m(x - C_m t, z) + \bar{w}_m(x - \bar{C}_m t, z)], \end{aligned}\right\} \tag{3.5}$$

	$A_0 = 4.807 \times 10^{-2}$	$\bar{A}_0 = 1.613 \times 10^{-3}, \omega_0 = 0.2607$		
m	A_m	C_m	$\bar{A}_m$	$\bar{C}_m$
1	2.247×10^{-2}	0.5621	4.554×10^{-3}	0.2027
2	1.260×10^{-2}	0.5621	6.110×10^{-3}	0.1836
3	6.597×10^{-3}	0.5621	5.825×10^{-2}	0.3154
4	3.934×10^{-3}	0.5621	4.520×10^{-2}	0.3710
5	2.526×10^{-3}	0.5621	1.795×10^{-2}	0.4192
6	6.055×10^{-3}	0.3158	5.656×10^{-3}	0.4448
7	4.042×10^{-3}	0.3524	2.531×10^{-3}	0.4569

		E_m		
$m = 0$	1	2	3	4
2.776×10^{-3}	2.752×10^{-4}	1.152×10^{-4}	1.604×10^{-3}	1.144×10^{-3}
5	6	7	8	9
1.806×10^{-4}	3.136×10^{-5}	9.076×10^{-6}	3.589×10^{-6}	2.682×10^{-6}
10	11	12	13	14
1.585×10^{-6}	9.124×10^{-7}	5.961×10^{-7}	2.663×10^{-7}	2.084×10^{-7}
15	16			
2.320×10^{-7}	2.297×10^{-7}			

TABLE 3. Values of the maximal amplitudes A_m, $\bar{A}_m$, phase velocities C_m, $\bar{C}_m$, frequency ω_0 in (3.2)–(3.4) and mode energies E_m for the two-dimensional secondary flow at $R_p = 2935$ and $\alpha_0 = 0.3387$ (run 30)

where u_0, u_m, $\bar{w}_m$ are even functions of the variable z and $\bar{u}_0$, $\bar{u}_m$, w_m are odd functions of z; $C_m = \omega_m/\alpha_m$, $\bar{C}_m = \bar{\omega}_m/\alpha_m, \alpha_m = m\alpha_0$.

Values of amplitudes $A_m = \max_s |A_{m,2s}|$ and $\bar{A}_m = \max_r |A_{m,2r+1}|$ as well as the phase velocities C_m, $\bar{C}_m$ for $m = 1, \ldots, 7$ and the frequency ω_0 are presented in table 3. Here the values of mode energies E_m for $m = 0, \ldots, 16$ are also presented. It is interesting to note that the phase velocity of the first five waves $\boldsymbol{V}_m = \{u_m, 0, w_m\}$ are equal to each other.

Thus the secondary flow under consideration consists of a large number of progressive waves propagating along the x-axis with different phase speeds. In addition $\langle \boldsymbol{V}(x,z,t)\rangle_x$ consists of an item that does not change in time and on which a standing wave with small amplitude is imposed.

We have also investigated the accuracy of the simulation of two-dimensional secondary flows. In run 30 at $R_p = 2935$, $\alpha_0 = 0.3387$ the secondary flow with $R_Q = 2723$ was obtained. By doubling the numbers M and P in the representations (2.12) of the approximate solution, we repeated the computation of the secondary flow. The integral characteristics of secondary flow Q and E_{tot} obtained in this repetition in fact coincided with those in run 30.

In the next control run at $R_p = 10^4$, $\alpha_0 = 1.25$, $(2M+1) \times (P+1) = 17 \times 65$ the spatial resolution in the x-direction in run 22 was doubled (see table 1). The changes in Q and E_{tot} were respectively 0.3 % and 0.8 % of their values.

Some computations with various time steps τ showed that our numerical technique allowed a rather large time step $\tau = 0.1$.

Finally note that a few secondary flows were computed repeatedly by means of some other numerical techniques. The changes arising in the secondary flows appeared to be insignificant.

Thus the control runs showed that the two-dimensional secondary flows were computed with a good accuracy. Some additional details on the two-dimensional secondary flows, their properties, accuracy, etc. may be found in Rozhdestvensky & Simakin (1982*b*, *c*, 1983) and Simakin (1983*b*).

4. Three-dimensional secondary flows and their comparison with turbulent flows†

In this section we present the results of computations of three-dimensional secondary flows in a plane channel. Again the mean-pressure gradient is fixed and we use the numerical method described in §2.

In all the three-dimensional runs $M = N = 4$ and $P = 32$, which corresponds to $3(2M+1)(2N+1)(P+1) = 8019$ degrees of freedom of the representation (2.12) of the velocity field in our numerical method. Some other parameters and results of the computations are given in table 4. Low values of M and N are used, because of the substantial increase in computer time needed with increase in M and N. We also were not able to carry out a considerable number of runs at various α_0 and β_0 in the three-dimensional case. These circumstances do not allow us to reach justified conclusions on limit secondary flows with maximal drag as in the two-dimensional case.

We think that such an investigation of the three-dimensional limiting secondary flows is useful, but it requires a cooperation of efforts in this direction.

The first three-dimensional secondary flow was computed at $R_p = 5000$ and $\alpha_0 = 1.25$, $\beta_0 = 2$ (see table 4). As the initial condition in this run the velocity field of the two-dimensional secondary flow with the same $R_p = 5000$ and $\alpha_0 = 1.25$ was taken on which a small three-dimensional disturbance $V_0(x, y, z)$ was imposed, where $u_0(x, y, z)$, $w_0(x, y, z)$ are even functions and $v_0(x, y, z)$ is an odd function of y. It may be easily shown that these properties of the velocity components, i.e. the y-symmetry of u, w and the y-antisymmetry of v, will be preserved in the flow for all $t > 0$. This flow passed to a steady regime with $R_Q = 2037$. Note that the reduction of the flow rate proportional to $R_p - R_Q$ increased by a factor of more than two as compared with the flow-rate reduction in the two-dimensional secondary flow.

The next run 2 was performed at the same parameters $R_p = 5000$, $\alpha_0 = 1.25$, $\beta_0 = 2$. However, in contrast with the previous run, here an initial three-dimensional disturbance $V_0(x, y, z)$ of a general form was imposed. This run was performed in the time interval $(0, 3000)$ up to the passage of the flow to a secondary regime. The principal integral characteristics $E_{\text{tot}}(t) = (1/2XY)\iiint_D V^2(X, t)\,dx\,dy\,dz$‡ and ΔQ_x of this secondary flow appeared to be sufficiently close to those obtained in the previous secondary flow (see table 4, runs 1, 2).

Departing from the three-dimensional secondary flow found at $R_p = 5000$, we gradually go over to other Reynolds numbers R_p. As an initial condition in the next runs the velocity field $V(X, T)$ transformed in a certain way was imposed which was obtained in the foregoing computation of the three-dimensional secondary flow. This technique of search reduces the time of passage of the flow to a steady regime. In this way three-dimensional secondary flows at $R_p = 7500$, 3500, 2800, 2100 were

† This part of our work had been completed by 1 February 1983 and was included in the revised version of our original manuscript. A very brief report on the results was given by Rozhdestvensky & Simakin (1983).

‡ Here the domain $D \equiv \{|x| \leqslant \frac{1}{2}X, |y| \leqslant \frac{1}{2}Y, |z| \leqslant 1\}$.

Run	Reynolds number R_p	Minimal wavenumbers α_0	β_0	Termination time of computation $T\times10^{-2}$	Reynolds number R_Q	Normalized flow rate Q/Q_0	Total energy of disturbances $E\times10$
1	5000	1.25	2.0	35	2037	0.407	2.159
2	5000	1.25	2.0	30	2023	0.405	2.162
3	5000	1.25	3.0	15	1958	0.392	2.232
4	5000	1.25	4.0	15	2080	0.416	2.097
5	7500	1.5	2.0	45	2585	0.345	2.514
6	3500	1.25	2.0	30	1665	0.476	1.767
7	2800	1.25	2.0	25	1498	0.535	1.594
8	2100	1.25	2.0	20	1313	0.625	1.008
9	1790	1.25	2.0	20	1790	1	0
10	1250	1.0	1.0	13	1250	1	0

TABLE 4. Characteristics of the three-dimensional computations of the evolution of finite-amplitude disturbances in plane Poiseuille flow

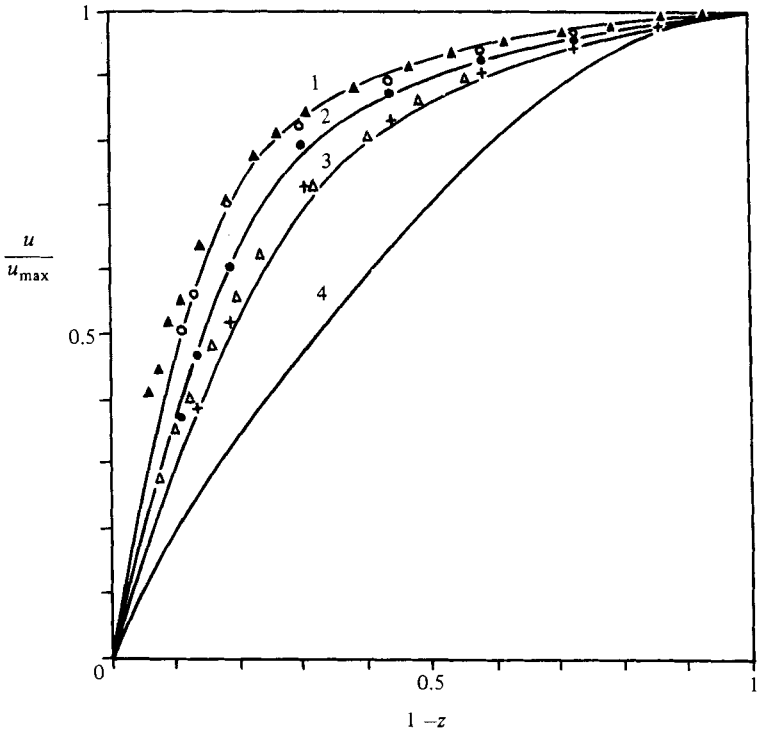

FIGURE 10. Normalized profiles of the mean velocity at various Reynolds numbers R_Q. Experimental results: ○, $R_Q = 2127$; ●, 1463; +, 1217 (Whan & Rothfus 1959); ▲, 2070, △, 1294 (Patel & Head 1969). Results of calculations: curve 1, $R_Q = 2037$ (3D, run 1); 2, 1498 (3D, run 7); 3, 1313 (3D, run 8); 4, mean-velocity profile in two-dimensional secondary flow at $R_Q = 2952$ (2D, run 8).

obtained. The flow in run 8 ($R_p = 2100$) passed to a steady regime with $R_Q = 1313$, but the evolution of disturbances in run 9 ($R_p = 1790$) resulted in their complete decay.

Thus for the Reynolds numbers $R_p \geqslant 2100$ ($R_Q \geqslant 1313$) the stable three-dimensional secondary flows in the plane channel were found. This implies the

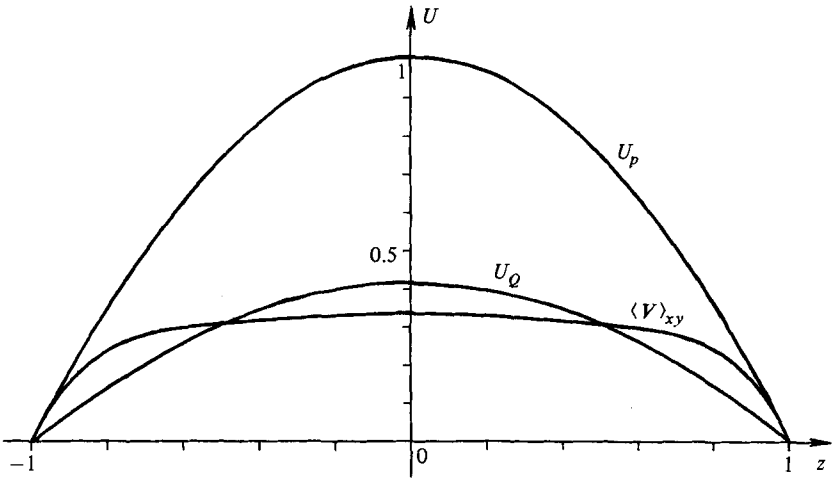

FIGURE 11. Mean velocity profiles $\langle V \rangle_{xy}$ of three-dimensional secondary flow at $R_p = 5000$, $R_Q = 2037$ (run 1), the velocity profile of Poiseuille flow $U_p(z)$ at $R = R_p = 5000$, the velocity profile of Poiseuille flow $U_Q(z)$ at $R = R_Q = 2037$.

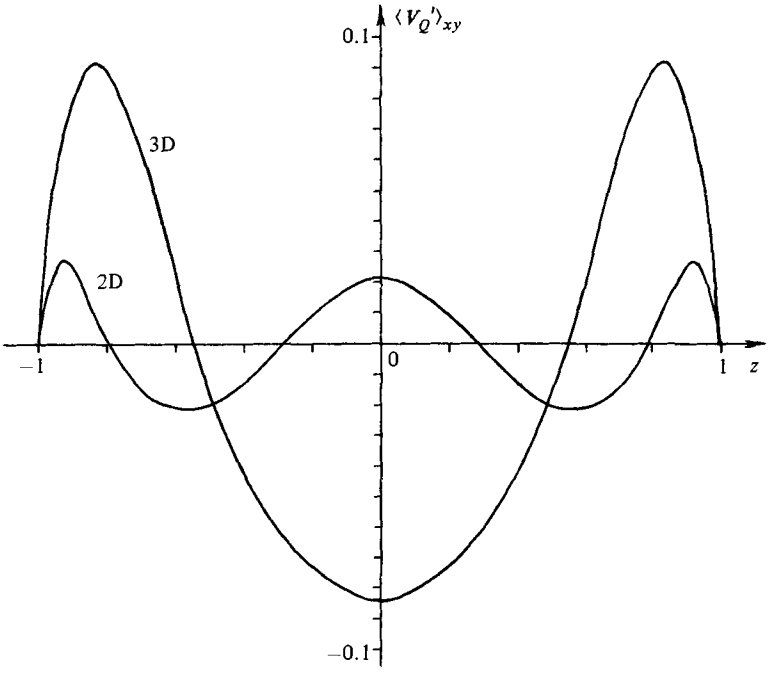

FIGURE 12. Results of recalculation of the mean-disturbance-velocity profiles of two-dimensional (run 5, table 1) and three-dimensional (run 1, table 4) secondary flows for another external condition, $Q = \text{const}$.

instability of the plane Poiseuille flow to finite-amplitude three-dimensional disturbances at these Reynolds numbers. This conclusion agrees rather well with the results of experiments by Davies & White (1928), Whan & Rothfus (1959), Patel & Head (1969) and Kao & Park (1970) in which transition to turbulence in the plane channel was observed for $R_Q \gtrsim 1000$.

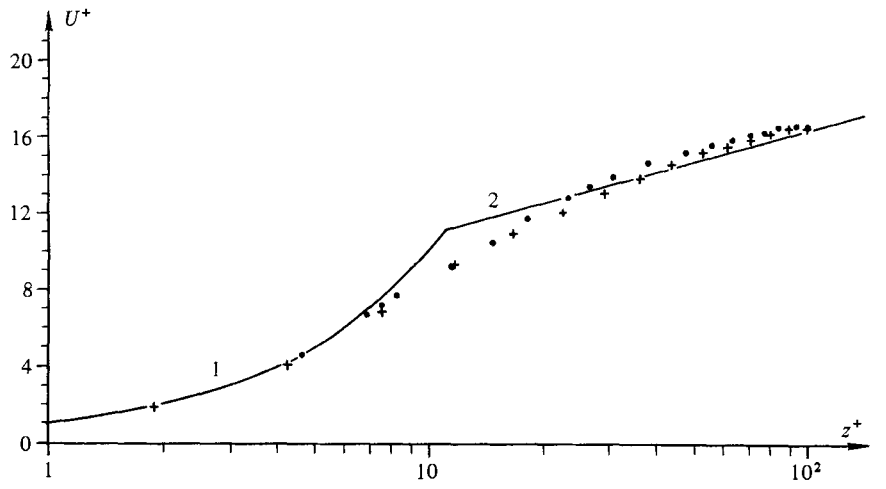

FIGURE 13. Mean-velocity profiles: ●, experimental results by Patel & Head (1969) at $R_Q = 2070$, +, the results of calculations in run 1 ($R_Q = 2037$, $R_p = 5000$, $\alpha_0 = 1.25$, $\beta_0 = 2$); curve 1, $U^+ = z^+$; 2, $U^+ = 5.5 \log_{10} z^+ + 5.45$. Here $U^+ = \langle V \rangle_{xy}/u_\tau$, $z^+ = zu_\tau/\nu$.

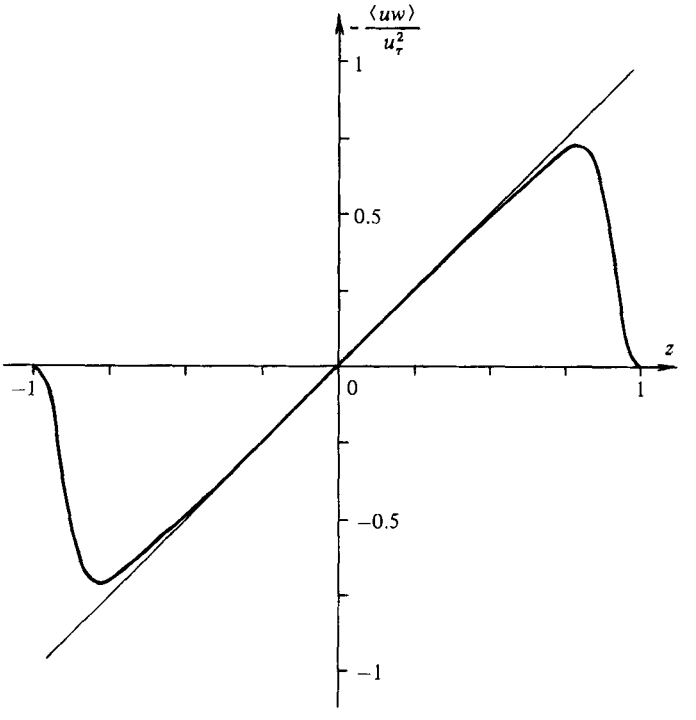

FIGURE 14. Reynolds stress for the three-dimensional secondary flow at $R_p = 5000$ (run 1).

The comparison of mean-flow velocity in the three-dimensional secondary flows with the experimental data by Whan & Rothfus (1959) and Patel & Head (1969) is presented in figure 10. We may say that beyond all our expectation agreement between mean-velocity profiles is very good. For contrast the mean-velocity profile in two-dimensional secondary flow at $R_Q = 2952$ ($R_p = 3500$) is also plotted (curve 4).

Figure 11 shows the mean-velocity profile $\langle V \rangle_{xy}$ in three-dimensional secondary

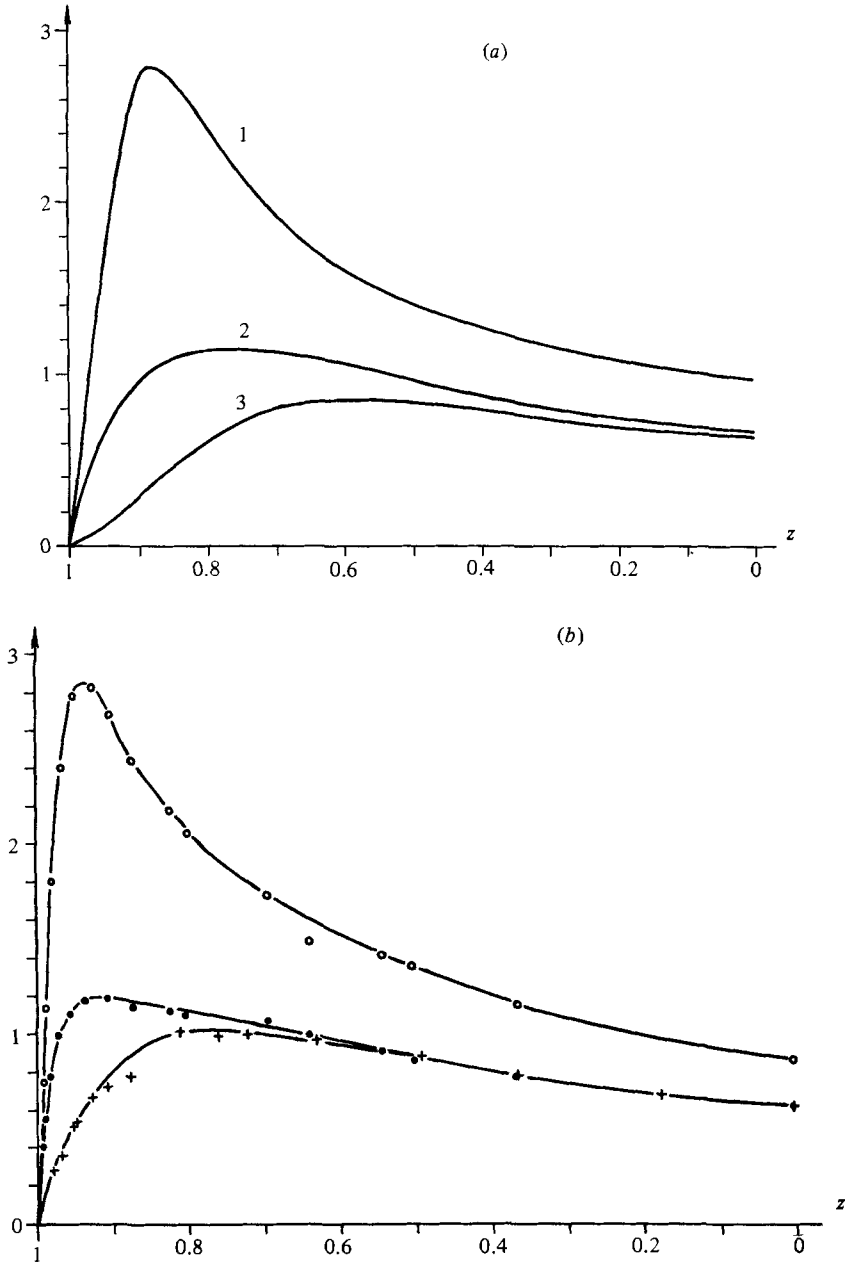

FIGURE 15. (*a*) Calculated distribution of the r.m.s. pulsation velocity components: curve 1, u; 2, v; 3, w as the functions of z at $R_p = 5000$, $R_c = \max_z \langle V \rangle_{xy}/\nu = 1620$ (run 2). (*b*) Experimental distribution of the r.m.s. pulsation velocity components: ○, u; ●, v; +, w as functions of z at $R_c = 3850$ (Kreplin & Eckelmann 1979).

flow ($R_p = 5000$, $R_Q = 2037$, $\alpha_0 = 1.25$, $\beta_0 = 2$), the velocity profile in Poiseuille flow at $R = R_p = 5000$, and the velocity profile in Poiseuille flow at $R = R_Q = 2037$.† In this figure for each problem formulation, i.e. for the flows with fixed flux ($R_Q = \text{const}$) and for the flows with fixed R_p, the typical relation between the profiles of the mean

† Here we fix the viscosity $\nu = 1/R_p$ and the half-channel width $L = 1$.

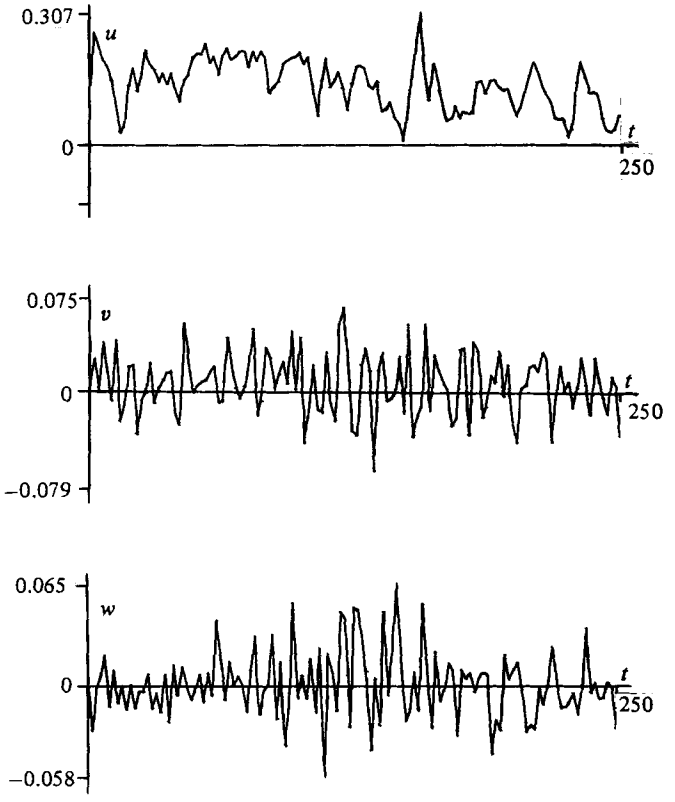

FIGURE 16. Behaviour of each component of the disturbance velocity of three-dimensional secondary flow at $R_p = 5000$ (run 2) over the time interval $t = 1700$–1950 at points $\{x = 0, y = \frac{1}{4}\pi, z = z_u, z_v, z_w\}$. The zeroth harmonic of the disturbance velocity is calculated as a deviation from the velocity in the Poiseuille flow at $R = R_Q = 2023$, and points z_u, z_v, z_w are close to those in which the amplitudes of pulsation of u, v, w are maximal.

velocity of the laminar and turbulent flows may be seen. In the experiments an analogous flattening of the mean-velocity profile is usually observed.

Figure 12 shows the mean-disturbance-velocity profiles at $R_p = 5000$, which are obtained as the deviations from the velocity in Poiseuille flow at $R_Q = 2037$ for three-dimensional secondary flow and from the velocity in Poiseuille flow at $R_Q = 3616$ ($R_p = 5000$, run 5, table 1) for two-dimensional secondary flow. We see that a 'three-humped' mean-disturbance-velocity profile appears only in two-dimensional secondary flows.

In figure 13 the mean-velocity profile in three-dimensional secondary flow at $R_p = 5000$ ($R_Q = 2037$), the same as in figure 11, is plotted as a function of $z^+ = zu_\tau/\nu$. Here the results by Patel & Head (1969) at $R_Q = 2070$ are also presented. Note the good agreement of the results of our computations with both experimental data and the 'universal wall law': $U^+ = z^+$ for $z^+ \lesssim 10$; $U^+ = 5.5 \log_{10} z^+ + 5.45$ for $z^+ \gtrsim 30$, where $U^+ = \langle V \rangle_{xy}/u_\tau$.

A plot of the Reynolds stress $-\langle uw \rangle_{xy}/u_\tau^2$ for three-dimensional secondary flow at $R_p = 5000$ is presented in figure 14. The maximum of the Reynolds stress occurs near the channel walls, which agrees with the experiments.

Figure 15(*a*) shows the distributions of the r.m.s. pulsation-velocity components (in wall units u_τ) versus z in three-dimensional secondary flow at $R_p = 5000$ (run 2,

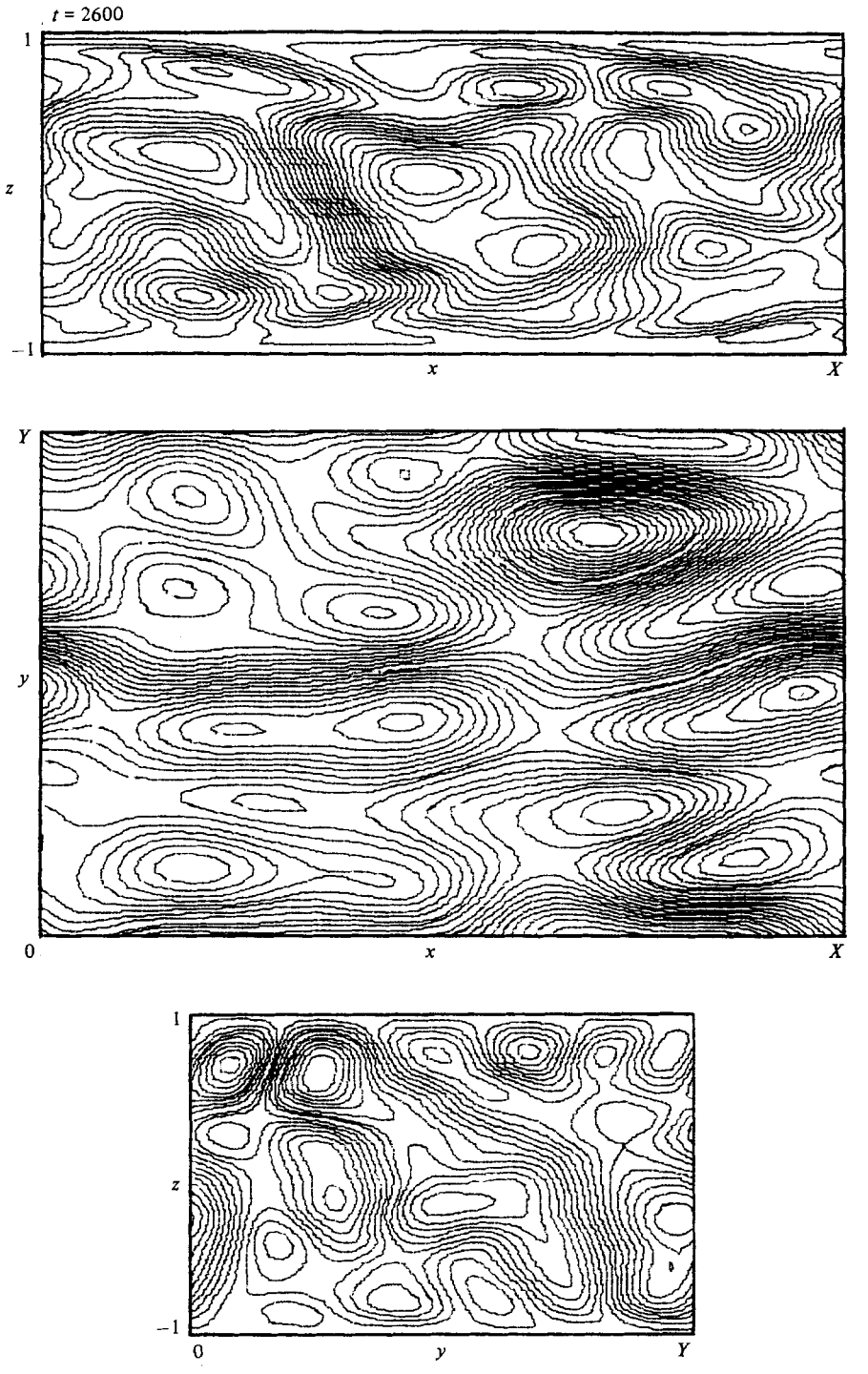

FIGURE 17. Instantaneous streamlines of the projections of the averaged vector fields $\langle \boldsymbol{V}' \rangle_y$, $\langle \boldsymbol{V}' \rangle_z$, $\langle \boldsymbol{V}' \rangle_x$ onto the planes $y = \text{const}$, $z = \text{const}$, $x = \text{const}$ respectively. Here $\boldsymbol{V}' = \boldsymbol{V} - \boldsymbol{V}_0$, $\boldsymbol{V}$ is the velocity field of the three-dimensional secondary flow at $R_p = 5000$ (run 2), $\boldsymbol{V}_0$ is the mean velocity of the flow.

$R_c = \max_z \langle V \rangle_{xy}/\nu = 1620$). The nearest Reynolds number R_c for which we were able to find the experimental data on these distributions was $R_c = 3850$ from Kreplin & Eckelmann (1979). We present the distributions of r.m.s. pulsation-velocity components from their work in figure 15(*b*). Comparison of figure 15(*a*) with 15(*b*) shows at least good qualitative agreement.

The behaviour in time of each component of the velocity in the run 2 ($R_p = 5000$) at points $\{x = 0, y = \frac{1}{4}\pi, z = z_u, z_v, z_w\}$ is presented in figure 16. These points z_u, z_v, z_w are close to those in which the amplitudes of pulsations of u, v, w are maximal. These graphs show that three-dimensional secondary flows are completely unlike time-periodic flows.

For the three-dimensional secondary flow (run 2) instantaneous streamlines of vector-field projections $\langle V' \rangle_y$, $\langle V' \rangle_z$, $\langle V' \rangle_x$ onto the planes $y = \text{const}$, $z = \text{const}$, $x = \text{const}$ respectively are depicted in figure 17. Here $\langle V' \rangle_y$, $\langle V' \rangle_z$, $\langle V' \rangle_x$ denote the averagings of the velocity field $V'(X,t) = V(X,t) - V_0(z)$ with respect to coordinates y, z, x respectively; V is the velocity field of the three-dimensional secondary flow considered, $V_0 = \langle V \rangle_{xy}$. An elimination of the mean velocity V_0 makes it possible to show the details of the considered averaged velocity fields. The projections presented give an idea of the eddies of the secondary flow.

Some remarks on the accuracy of our computations of three-dimensional secondary flows are given in §5.

5. Discussion and comparison of the results

The secondary flows that we have obtained imply the instability of the Poiseuille flow to finite disturbances. Such a disturbance may be, for example, $V(X,t) - U_0(z)$, where V and U_0 are respectively the velocity fields of the secondary flow at arbitrary moment of time t and of the Poiseuille flow.

For the present we are interested mainly in the existence and properties of secondary flows as well as their relation to the turbulence. The conditions for passage of the flow to a secondary regime are of course also interesting, but here we pay less attention to them.

First of all we note that in our investigations the quantities α_0 and β_0 are far from always being the wavenumbers of the unique mode of the initial disturbance, but $X = 2\pi/\alpha_0$, $Y = 2\pi/\beta_0$ are always the periodicity intervals of the secondary flow in homogeneous coordinates (x, y).

In such an understanding of the functions of the parameters α_0 and β_0 the so-called 'neutral surface' in the theory of nonlinear stability will describe many more statistically stationary solutions of Navier–Stokes equations. In fact, any solution $V(X,t)$ periodic in x with a period $X = 2\pi/\alpha_0$ is also periodic in x with the periods $X_m = mX = 2\pi/\alpha_{0m}$, $\alpha_{0m} = \alpha_0/m$, $m = 2, 3, \ldots$. Therefore, if the point (α_0, β_0) belongs to the neutral surface then all the points $(\alpha_{0m}, \beta_{0n})$ must also belong to it. It is rather obvious, and our calculations confirm, that the solution $V(X,t)$ mentioned above is unstable to periodic disturbances with the periods mX, nY. As a result of the evolution of these long-wave disturbances we obtain another secondary flow at α_{0m}, β_{0n} which must also belong to the neutral surface. It seems to us that this simple observation may be useful for the explanation of the existence of the long-wave secondary flows at the Reynolds numbers at which the short-wave secondary flows do not exist or are unstable.

A secondary flow with the periods $X = 2\pi/\alpha_0$, $Y = 2\pi/\beta_0$ can sometimes be obtained as a result of the evolution of the initial harmonic disturbance with the

wavenumbers α_0 and β_0 and sometimes cannot. Full elucidation of this question requires a great amount of computer time. Note that in the most part of works devoted to investigation of nonlinear stability of Poiseuille flow this question is also left without an answer.

The calculations of two-dimensional secondary flows performed on considerably large time intervals $T \sim 10^4$ have not led to the passage of these flows to the time-periodic regimes. Nevertheless two-dimensional secondary flows are rather similar to the time-periodic ones, especially for $\alpha_0 > 1$ and large Reynolds numbers.

Our main conclusion from two-dimensional computations is that two-dimensional solutions of the Navier–Stokes equations can determine correctly neither the critical Reynolds number of transition to turbulence nor very important parameters of turbulent flows. Such a conclusion is apparently in accordance with the modern point of view on this question.

Some of our discrepancies with results by other authors in two-dimensional instability of plane Poiseuille flow are related to the small 'transition' zone $R_p = 2700$–3250, i.e. to the margin of the domain of the existence of two-dimensional secondary flows. Here we were not able to find a secondary flow with $\alpha_0 \gtrsim 1$, but have found them for $\alpha_0 \lesssim 0.3$.

As an example we compare our results on two-dimensional secondary flows with those by Zahn *et al.* (1974). Their UB-solutions agree qualitatively and sometimes quantitatively rather well with our solutions except for the transition zone. Discrepancies of UB-solutions with our data for two-dimensional secondary flows are apparently explained by an insufficient accuracy of their simple one- and two-mode models. This is attested in particular by their own computations at $R_p = 10^4$, $\alpha_0 = 1$. In their case I (one-mode model) the flow rate $Q = 0.746$, in case II (two-mode model) $Q = 0.846$. A passage from one to two modes leads to a more than 11 % change in the flow rate and about 22 % change in the drag coefficient. In our calculations at the same parameters $Q = 0.926$.

Further it is necessary to give some critical comments on the papers by Orszag & Kells (1980) and Orszag & Patera (1980, 1981, 1983), since in the case of plane Poiseuille flow the purposes and even the methods of their and our investigations are rather close. They employed the effective numerical technique of Orszag & Kells, but in all their computations the integration times were very small: $T \leqslant 150$ and $T \leqslant 75$ for two- and three-dimensional cases respectively. Based on these short computations, Orszag & Kells made conclusions on the stability and instability of the plane Poiseuille flow. No secondary regimes of flow were obtained by them. Our repetitions and prolongations of all their 'successful' two-dimensional runs (i.e. the runs which by Orszag & Kells testify the instability of the Poiseuille flow) have led to the opposite conclusion. In these runs we made use of their own numerical technique and had to increase the integration times by factors of 20–50. Further details on this question can be found in Rozhdestvensky & Simakin (1982*b*, *c*).

After this it was obvious that all three-dimensional computations by Orszag & Kells and Orszag & Patera had the same shortcoming, which may affect their conclusions on 'breakdown to turbulence', turbulent mean-velocity profiles, etc.

Thus the papers we know contain almost nothing that could be compared directly with our three-dimensional secondary flows. For this reason we confine ourselves only to comparisons of our three-dimensional results with the experimental data.

Finally let us discuss the accuracy of our three-dimensional computations. First of all we have to say that the resolution in the z-direction is not too bad, and $P = 32$ is large enough for the first computations. However the resolution in the x- and

	E_{mn}				
m \ n	0	1	2	3	4
0	2.148×10^{-1}	2.399×10^{-4}	2.034×10^{-4}	5.283×10^{-5}	6.490×10^{-5}
1	2.934×10^{-5}	8.440×10^{-5}	1.591×10^{-4}	9.718×10^{-5}	8.142×10^{-5}
2	2.259×10^{-5}	4.806×10^{-5}	3.846×10^{-5}	3.744×10^{-5}	3.167×10^{-5}
3	1.699×10^{-5}	3.444×10^{-5}	2.065×10^{-5}	2.510×10^{-5}	2.680×10^{-5}
4	8.897×10^{-6}	1.834×10^{-5}	2.085×10^{-5}	2.053×10^{-5}	1.854×10^{-5}

TABLE 5. Values of the mode energies E_{mn} at the end of the three-dimensional run 2 ($R_p = 5000$, $\alpha_0 = 1.25$, $\beta_0 = 2$)

y-directions is far from being as good as in two-dimensional computations. With $M = N = 4$ all the 24 modes allowed in the representation of numerical solution corresponding to subscripts m, n ($m^2 + n^2 \neq 0$) have among themselves comparable energies. In table 5 are presented their energies at the end of run 2 ($R_p = 5000$). The diminution of E_{mn} for $m = 4$ and for $n = 4$ is roughly by factors of 0.3–0.1. These factors are better for run 4 ($\beta_0 = 4$).

Thus the resolution in the x- and y-directions is insufficient, and, strictly speaking, this method of obtaining three-dimensional secondary flows with $M = N = 4$ may be called 'the 24-mode model'. But it can be used for numerical computation of three-dimensional secondary flows if we increase M and N appreciably. This work is planned.

Nevertheless, it is a fact that this '24-mode model' reflects the basic integral properties of turbulent flows rather well at moderately large Reynolds numbers, and we are sure that this is not fortuitous. Moreover it strengthens our conviction that among the infinite set of three-dimensional secondary flows (and, corresponding to them, solutions of the Navier–Stokes equations) there exist secondary flows that completely describe the real turbulent imcompressible fluid flows in the channels and pipes.

The authors express their deep gratitude to Academicians A. A. Samarsky, A. N. Tichonov and the late N. N. Yanenko for the essential support of this work. The authors also thank their colleague V. G. Priymak for assistance in the work and Professor V. Ya. Shkadov for numerous discussions of various aspects of this paper.

REFERENCES

BETCHOV, R. & CRIMINALE, W. O. 1967 *Stability of Parallel Flow*. Academic Press.

DAVIES, S. J. & WHITE, C. M. 1928 An experimental study of the flow of water in pipes of rectangular section. *Proc. R. Soc. Lond.* A **119**, 92–107.

DRAZIN, P. G. & REID, W. H. 1981 *Hydrodynamic Stability*. Cambridge University Press.

FOX, L. 1962 Chebyshev methods for ordinary differential equations. *Comp. J.* **4**, 318–331.

GEORGE, W. D., HELLUMS, J. D. & MARTIN, B. 1974 Finite-amplitude neutral disturbances in plane Poiseuille flow. *J. Fluid Mech.* **63**, 765–771.

GOLDSHTIK, M. A. & STERN, V. N. 1977 *Hydrodynamic Stability and Turbulence*. Novosibirsk, Nauka.

GOTTLIEB, D. & ORSZAG, S. A. 1977 Numerical analysis of spectral methods: theory and applications. *SIAM, NSF–CBMS Monograph* 29.

HERBERT, T. 1977 Finite amplitude stability of plane parallel flows. In *Proc. AGARD Symp. on Laminar–Turbulent Transition* no. 3.

HERBERT, T. 1983 On perturbation methods in nonlinear stability theory. *J. Fluid Mech.* **126**, 167–186.

JOSEPH, D. D. 1976 *Stability of Fluid Motions I, II.* Springer.

KAO, T. W. & PARK, C. 1970 Experimental investigation of the stability of channel flows. Part 1. Flow of a single liquid in rectangular channel. *J. Fluid Mech.* **43**, 145–164.

KAPORIN, I. E. 1980 New fast Fourier transform algorithm. *Zh. Vychisl. Mat. i Mat. Fiz.* **20**, 1054–1058.

KREPLIN, H. & ECKELMANN, M. 1979 Behaviour of the three fluctuating velocity components in the wall region of a turbulent channel flow. *Phys. Fluids* **22**, 1233–1239.

LANCZOS, C. 1956 *Applied Analysis.* Prentice-Hall.

MOIN, P. & KIM, J. 1980 On the numerical solution of time-dependent viscous incompressible fluid flows involving solid boundaries. *J. Comp. Phys.* **35**, 381–392.

ORSZAG, S. A. 1971 Numerical simulation of incompressible flows within simple boundaries. I. Galerkin (spectral) representations. *Stud. Appl. Maths* **50**, 293–327.

ORSZAG, S. A. & KELLS, L. C. 1980 Transition to turbulence in plane Poiseuille and plane Couette flows. *J. Fluid Mech.* **96**, 159–205.

ORSZAG, S. A. & PATERA, A. T. 1980 Subcritical transition to turbulence in plane channel flows. *Phys. Rev. Lett.* **45**, 989–993.

ORSZAG, S. A. & PATERA, A. T. 1981 Calculation of von Kármán's constant for turbulent channel flow. *Phys. Rev. Lett.* **47**, 832–835.

ORSZAG, S. A. & PATERA, A. T. 1983 Secondary instability of wall-bounded shear flows. *J. Fluid Mech.* **128**, 347–385.

PATEL, V. C. & HEAD, M. R. 1969 Some observations on skin friction and velocity profiles in fully developed pipe and channel flows. *J. Fluid Mech.* **38**, 181–201.

PETROV, G. I. 1940 The application of the Galerkin method to the problem of stability of viscous fluid flow. *Prikl. Mat. i Mekh.* **4**, 3–12.

ROZHDESTVENSKY, B. L. 1973 On the applicability of finite-difference methods to the solution of Navier–Stokes equations at large Reynolds numbers. *Dokl. Akad. Nauk SSSR* **211**, *308–311.*

ROZHDESTVENSKY, B. L., ERMAKOVA, E. I. & PRIYMAK, V. G. 1977 A study of the stability of difference schemes of higher order accuracy. *Keldysh Inst. Appl. Maths Preprint* 14.

ROZHDESTVENSKY, B. L. & PRIYMAK, V. G. 1982 Numerical simulation of two-dimensional turbulence in a plane channel. *Comp. Fluids* **10**, 117–126.

ROZHDESTVENSKY, B. L. & SIMAKIN, I. N. 1982*a* Methods of numerical simulation of unsteady flows of incompressible viscous fluid in a plane channel. *Keldysh Inst. Appl. Maths Preprint* 191.

ROZHDESTVENSKY, B. L. & SIMAKIN, I. N. 1982*b* Nonstationary secondary flows in a plane channel and stability of the Poiseuille flow with respect to finite disturbances. *Dokl. Akad. Nauk SSSR* **266**, 1337–1340.

ROZHDESTVENSKY, B. L. & SIMAKIN, I. N. 1982*c* Stability of the Poiseuille flow with respect to finite disturbances. *Chisl. Metody Mekh. Sploshnoy Sredy, Novosibirsk* **13**, 89–128.

ROZHDESTVENSKY, B. L. & SIMAKIN, I. N. 1983 Two- and three-dimensional secondary flows in a plane channel, their relationship and comparison with turbulent flows. *Dokl. Akad. Nauk SSSR* **273**, 553–558.

ROZHDESTVENSKY, B. L. & YANENKO, N. N. 1978 *Systems of Quasi-Linear Equations.* Moscow, Nauka [English transl. *Am. Math. Soc. Monograph* 55 (1983)].

SAMARSKY, A. A. 1977 *Theory of Difference Schemes.* Moscow, Nauka.

SERRIN, J. 1959 Mathematical principles of classical fluid mechanics. In *Handbuch der Physik*, Bd. VIII/1 (ed. S. Flügge & C. Truesdell). Springer.

SHKADOV, V. YA. 1973*a* Some methods and problems of the hydrodynamic stability theory. *Nauch. Trudy Inst. Mekh. Moscow Univ.* 25.

SHKADOV, V. YA. 1973*b* On nonlinear evolution of the disturbances in plane-parallel Poiseuille flow. *Izv. Akad. Nauk SSSR, Mekh. Zhid. i Gaza* no. 2, pp. 49–57.

SIMAKIN, I. N. 1983*a* Investigation of the stability and accuracy of the methods of numerical simulation of nonstationary flows in a plane channel. *Keldysh Inst. Appl. Maths Preprint* 49.

SIMAKIN, I. N. 1983*b* Numerical investigation of the accuracy of simulation of unsteady flows in a plane channel. *Keldysh Inst. Appl. Maths Preprint* 60.

STEWARTSON, K. 1974 Some aspects of nonlinear stability theory. *Fluid Dyn. Trans.* **7**, 101–128.

STUART, J. T. 1960 On the non-linear mechanics of wave disturbances in stable and unstable parallel flows. Part I. The basic behaviour in plane Poiseuille flow. *J. Fluid Mech.* **9**, 353–370.

STUART, J. T. 1971 Non-linear stability theory. *Ann. Rev. Fluid Mech.* **3**, 347–370.

THOMAS, T. Y. 1942 Qualitative analysis of the flow of fluids in pipes. *Am. J. Maths* **64**, 754.

WHAN, G. A. & ROTHFUS, R. R. 1959 Characteristics of transition flow between parallel plates. *A.I.Ch.E J.* **5**, 204–208.

YANENKO, N. N. 1967 *Fractional Steps Method of the Solution of Many-dimensional Problems in Mathematical Physics*. Novosibirsk, Nauka.

ZAHN, J.-P., TOOMRE, J., SPIEGEL, E. A. & GOUGH, D. O. 1974 Nonlinear cellular motions in Poiseuille channel flow. *J. Fluid Mech.* **64**, 319–345.